

## Hyperfine-Structure Measurements of Excited $S$ States of the Stable Isotopes of Potassium, Rubidium, and Cesium by Cascade Radio-Frequency Spectroscopy\*

R. Gupta, W. Happer, L. K. Lam, and S. Svanberg<sup>†‡</sup>

Columbia Radiation Laboratory, Department of Physics, Columbia University, New York, New York 10027

(Received 6 August 1973)

The hyperfine structure of several of the excited  $S$  states of the stable isotopes of potassium, rubidium, and cesium has been measured by the method of cascade radio-frequency spectroscopy. We find, for the magnetic dipole coupling constant  $A$ , in MHz, for  $K^{39}$ :  $A(5^2S_{1/2}) = 55.50(60)$ ,  $A(6^2S_{1/2}) = 21.81(18)$ ; for  $K^{41}$ :  $A(5^2S_{1/2}) = 30.75(75)$ ,  $A(6^2S_{1/2}) = 12.03(40)$ ; for  $Rb^{85}$ :  $A(6^2S_{1/2}) = 239.3(1.2)$ ,  $A(7^2S_{1/2}) = 94.00(64)$ ,  $A(8^2S_{1/2}) = 45.5(2.0)$ ; for  $Rb^{87}$ :  $A(6^2S_{1/2}) = 809.1(5.0)$ ,  $A(7^2S_{1/2}) = 318.1(3.2)$ ,  $A(8^2S_{1/2}) = 158.0(3.0)$ ; for  $Cs^{133}$ :  $A(7^2S_{1/2}) = 546.3(3.0)$ ,  $A(8^2S_{1/2}) = 218.9(1.6)$ , and  $A(9^2S_{1/2}) = 109.5(2.0)$ .

### I. INTRODUCTION

In this article we present extensive new results of hyperfine-structure (hfs) measurements on a total of thirteen excited  $S$  states of the stable isotopes of potassium, rubidium, and cesium by the method of cascade radio-frequency spectroscopy. Since the advent of optical double resonance<sup>1</sup> and level-crossing spectroscopy,<sup>2</sup> extensive measurements of the atomic parameters (e.g., hyperfine structures and lifetimes) of the excited  $P$  states of alkali-metal atoms have been performed.<sup>3</sup> These measurements have significantly increased our knowledge of atomic interactions, for example, of core polarization, electric quadrupole shielding, etc. However, until very recently no such measurements had been performed on the excited  $S$  states of the alkali metals, because of the difficulties in producing polarized excited  $S$  states. The Columbia group has recently demonstrated<sup>4-6</sup> that the excited  $S$  states can conveniently be populated by cascade excitation. Their preliminary investigations on the non- $P$ -states have already revealed some very interesting effects. For example, the hyperfine structure of the  $5^2D_{5/2}$  state of rubidium is found to be inverted, while that of the  $5^2D_{3/2}$  state is normal.<sup>5</sup> This may be related to the anomalously narrow fine structures of this state. The  $S$ -state hyperfine structure should be particularly interesting, as the hfs measurement should directly give the electron spin density at the nucleus. Although the hfs in the low-lying states of the alkali-metal atoms is principally due to a single valence electron, core-polarization effects can have a very significant effect on the hfs. It is not possible to determine the contribution of the core-polarization effects to the hfs in the  $^2S_{1/2}$  states from the measured hfs values alone. However, comparison of the measured hfs values with various theoretical val-

ues can give information on the effects of the core. Recently, Rosén and Lindgren<sup>7</sup> have calculated the values of the hfs intervals in the excited  $S$  states of alkali-metal atoms using restricted self-consistent-field methods. Comparison of these values with our measured values should give an estimate of the core polarization and other correlation effects in these states. We hope that our measurements will stimulate further theoretical work on the excited  $S$  states of alkali-metal atoms.

With few exceptions, all excited  $S$  states of alkali-metal atoms have hfs intervals that are small in comparison to the Doppler width of the spectral lines. Therefore, only high-resolution techniques, such as optical double resonance, which are primarily limited by the natural radiative linewidth, are suitable for an investigation of these states. Unfortunately, the  $S$  states cannot be populated by direct optical excitation of the ground-state atoms, as the selection rules for electric dipole radiation prohibit these transitions. Stepwise excitation, where a  $P$  state may be used as an intermediate state, is in principle possible but difficult with conventional lamps.<sup>8</sup> Recently, Svanberg *et al.*<sup>9</sup> have used stepwise excitation using a tunable cw dye laser in the second step to study some highly excited  $D$  and  $F$  states in rubidium and cesium. However, with the presently available wavelength range of tunable cw dye lasers, only relatively highly excited  $S$  states can be reached by this method. Recently we have reported<sup>6</sup> cascade-decoupling measurements of the hfs intervals in the second excited  $S$  states of  $K^{39}$  and  $K^{41}$  and in the second and third excited  $S$  states of  $Rb^{85}$ ,  $Rb^{87}$ , and  $Cs^{133}$ . In these measurements, the  $S$  states are populated by spontaneous decay of the highly excited  $P$  states. The hfs intervals are measured by observing the decoupling of the electronic and nuclear angular momenta in an external magnetic field. Although these rela-

tively rough values are useful, more accurate measurements are clearly desirable. Moreover, no attempts were made at that time to measure the hfs intervals in the *first* excited S states of alkali-metal atoms for reasons that will become clear below. Although the decoupling method is simple and has several advantages over rf spectroscopy,<sup>5,6</sup> the precision that can be achieved using this method is rather limited. Also, unless extreme care is taken, such systematic effects as the collisional depolarization of the excited states, nonwhite excitation, and Zeeman scanning of the absorption lines, etc., can give rise to additional uncertainties. We have recently reported our preliminary measurements of the hfs intervals in the  $7^2S_{1/2}$  state of rubidium<sup>5</sup> using radio-frequency spectroscopy in conjunction with cascade excitation. rf spectroscopy<sup>10</sup> is relatively free of large systematic effects, and greater precision in the hfs measurements can easily be obtained.

Our method for the case of the  $7^2S_{1/2}$  state of rubidium is schematically illustrated in Fig. 1. The third-resonance lines (3587 and 3592 Å) from a rubidium lamp are used to excite the Rb atoms to the  $7^2P_{1/2}$  and  $7^2P_{3/2}$  states. Atoms in these states can decay to all lower-lying S and D states, and there is a branching ratio of about 25% to the  $7^2S_{1/2}$  state. If circularly polarized uv exciting light is used, part of the photon's angular momentum is transferred into the electronic polarization

of the  $7P$  state. When the  $7P$  state decays to the  $7S$  state, part of the electronic polarization is carried over to the  $7^2S_{1/2}$  state. The  $7^2S_{1/2}$  state consequently achieves a certain degree of longitudinal electronic polarization. The 7408-Å fluorescent light which is emitted when the  $7^2S_{1/2}$  state decays to the  $5^2P_{3/2}$  level has a circular polarization proportional to the electronic polarization of the  $7^2S_{1/2}$  state. Thus, by observing the circular polarization of the 7408-Å (or 7280-Å) fluorescent light, one can monitor the electronic polarization of the  $7^2S_{1/2}$  state. In the presence of hfs, the  $7^2S_{1/2}$  state is split into two components, as shown in Fig. 2, for the case of Rb<sup>87</sup> (nuclear spin  $I = \frac{3}{2}$ ). When an external magnetic field is applied, the two hyperfine levels further split into magnetic sublevels, as shown. If radio-frequency transitions are now induced between a pair of sublevels, the populations of the two sublevels tend to equalize, resulting in a decrease in the electronic polarization of the  $7^2S_{1/2}$  state. This change can be detected by observing a decrease in the polarization of the 7408-Å fluorescent light. The hfs of the state is deduced from the measurement of the external magnetic field at which a given transition is observed.<sup>11</sup> The 7408-Å fluorescent light also carries information on the polarization in the  $7P$  state. Consequently, if rf transitions are induced in the  $7P$  state, they can also be observed as a change in the polarization of the 7408-Å fluores-

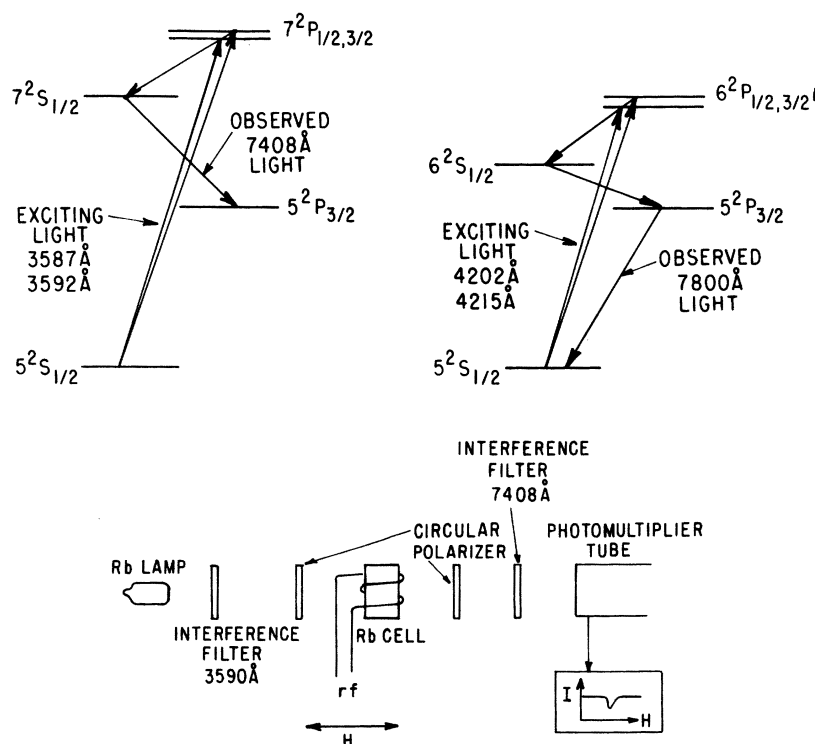


FIG. 1. Schematic illustration of the method of cascade radio-frequency spectroscopy. The polarized P states are created by excitation with circularly polarized resonance light. The excited S states are populated and polarized by the spontaneous decay of these P states. The polarization of the excited S states is monitored by observing the circular polarization of the fluorescent light. rf resonances in these states are observed as a decrease in the polarization of the fluorescent light.

cent light.

The scheme for investigating the hfs of the first excited S state of rubidium ( $6^2S_{1/2}$ ) is also shown in Fig. 1. The fluorescent light which is emitted when the  $6^2S_{1/2}$  state decays to the  $5P$  state lies well in the infrared region of the spectrum (about  $13\,000\text{ \AA}$ ) and cannot be detected by conventional photomultiplier tubes. Therefore we observe the polarization of the  $7800\text{-\AA}$  fluorescent light, which is emitted in the final step of the cascade process.<sup>12</sup> The rf resonances in the  $6^2S_{1/2}$  state can still be observed as a decrease in the polarization of the  $7800\text{-\AA}$  light, although the magnitude of the signal is somewhat degraded due to an additional step of cascading.

The experimental arrangement that we have used is simple and is shown schematically in Fig. 1 for the case of the  $7^2S_{1/2}$  state of rubidium. The third-resonance lines from a rubidium lamp are selected by an interference filter, pass through a circular polarizer, and are incident on a Pyrex cell containing rubidium vapor. The Rb cell is placed in a longitudinal static magnetic field, and a rf magnetic field perpendicular to the static field is applied. The  $7408\text{-\AA}$  fluorescent light is selected by an interference filter, analyzed for circular polarization, and detected by a photomultiplier tube. As the external static magnetic field is swept through the resonance, a sharp decrease in the intensity of the polarized fluorescent light is seen.

In the next section we will give the basic theory of the experiment. The details of the apparatus will be described in Sec. III; the results will be presented in Sec. IV; and a brief discussion of the results will be given in Sec. V.

## II. THEORY

In discussing the theory of these experiments we shall make extensive use of the theoretical section of Ref. 6, which we shall designate by GCH, and wherever possible we shall make use of well-established results from the theory of radio-frequency spectroscopy without rederiving them. We shall begin with a discussion of the basic observable of our experiments, the fluorescent light.

### A. Fluorescent Light

The intensity  $\Delta I$  of fluorescent light emitted into a small solid angle  $\Delta\Omega$  when an atom decays spontaneously from a state  $b$  to a state  $f$  is<sup>6</sup>

$$\Delta I = \text{Tr}[\rho_b \mathcal{L}] \Delta\Omega, \quad (1)$$

where  $\rho_b$  is the density matrix of the state  $b$  and the fluorescent-light operator is

$$\mathcal{L} = \frac{e^2 \omega_{bf}}{2\pi m^2 c^3 \hbar} \sum \hat{u} \cdot \hat{p} |f\nu\rangle \langle f\nu| \hat{u}^* \cdot \hat{p}. \quad (2)$$

Here  $\hat{u}$  is the polarization vector of the fluorescent light,  $\hat{p}$  is the momentum operator of the atom, and the sum in (2) extends over a complete set of sublevels  $|f\nu\rangle$  of the state  $f$ . If all hyperfine components of the fluorescent light are observed with equal efficiency, one can show that the fluorescent-light operator (2) can be written in the form

$$\mathcal{L} = \mathcal{L}_0 + \mathcal{L}_1 \vec{t} \cdot \vec{J} + \mathcal{L}_2 U_2 \cdot T_2(J_b J_b). \quad (3)$$

Explicit formulas for the constants  $\mathcal{L}_0$ ,  $\mathcal{L}_1$ , and  $\mathcal{L}_2$  follow from Eq. (13) of GCH. The mean spin of the fluorescent photons is  $\vec{t}$ ;  $\vec{J}$  is the electronic angular momentum operator of the atom;  $T_{2M}(J_b J_b)$  is the quadrupole basis operator, defined by Eq. (7) of GCH; and  $U_{2M}$  is a quadrupole polarization tensor, constructed from the polarization vector  $\hat{u}$  according to Eq. (8) of GCH.

In all of our experiments we use a rotating quarter-wave plate in the path of the detected fluorescent light (see Fig. 6). The rotating quarter-wave plate provides a low reference frequency  $\Omega$  for the lock-in amplifier, and it also makes the quantities  $t_x$  and  $U_{2\pm 2}$  of (3) oscillate at the reference frequency  $\Omega$ . The quantities  $t_x$ ,  $t_y$ , and  $U_{2\pm 1}$  are zero for our geometry (the  $z$  axis is parallel to the static magnetic field and also to the fluorescent light beam). Consequently the signal recorded by the lock-in amplifier will be a linear combination of  $\langle J_x \rangle$  and  $\langle T_{2\pm 2}(J_b J_b) \rangle$ . However, for sufficiently large static magnetic fields,

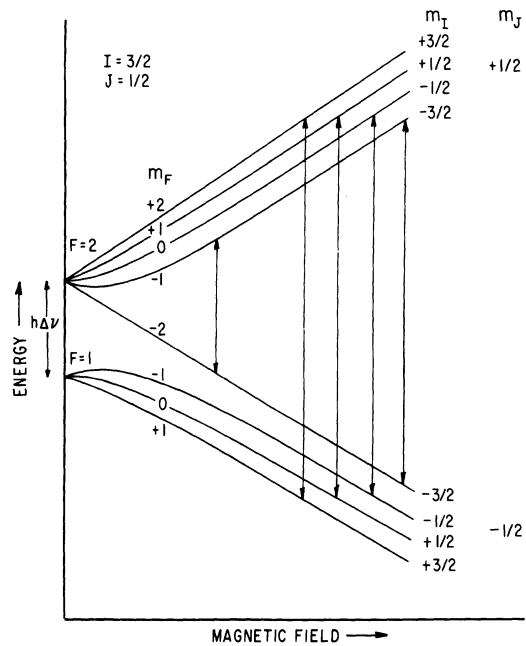


FIG. 2. Breit-Rabi diagram of a  $2S_{1/2}$  state for an atom with nuclear spin  $I = \frac{3}{2}$ . The vertical lines show some of the  $\Delta m = \pm 1$  transitions that we have observed.

the transverse polarization  $\langle T_{2\pm 2}(J_y J_y) \rangle$  will be negligibly small because of magnetic depolarization (the Hanle effect). In addition, if our exciting light were completely circularly polarized, and we attempt to make it so, no transverse polarization would be present at any magnetic field. Consequently, under our experimental conditions, we expect the lock-in amplifier to detect a signal proportional to  $\langle J_x \rangle$ , the mean electronic angular momentum of the fluorescing state. The goal of our theory is to predict the changes in  $\langle J_x \rangle$  produced by static and radio-frequency magnetic fields.

### B. Evolution of an Excited Atomic State

The evolution of an atom within an excited atomic state can be represented satisfactorily by the effective Hamiltonian

$$\mathcal{H} = \mathcal{H}_0 + V \cos \omega t, \quad (4)$$

where the static Hamiltonian is<sup>6</sup>

$$\mathcal{H}_0 = \hbar A \vec{I} \cdot \vec{J} + \hbar B \left( \frac{3(\vec{I} \cdot \vec{J})^2 + \frac{3}{2}(\vec{I} \cdot \vec{J}) - I(I+1)J(J+1)}{2I(2I-1)J(2J-1)} \right) + g_J \mu_B H J_x + g_I \mu_B H I_x, \quad (5)$$

and the interaction with an oscillating external magnetic field of magnitude  $H_1$  is

$$V = \mu_B \vec{H}_1 \cdot (g_J \vec{J} + g_I \vec{I}). \quad (6)$$

The term involving  $g_I$  in (6) can ordinarily be ignored, since it is three orders of magnitude smaller than the term involving  $g_J$ .

The static Hamiltonian  $\mathcal{H}_0$  will define a set of eigenstates  $|i\rangle$  with energies  $E_i$ ,

$$\mathcal{H}_0 |i\rangle = E_i |i\rangle. \quad (7)$$

The evolution of the excited-state density matrix is governed by the Liouville equation

$$\frac{d}{dt} \rho = \frac{1}{i\hbar} [\mathcal{H}_0, \rho] - \Gamma \rho + S + [V, \rho] \cos \omega t, \quad (8)$$

where  $\Gamma$  is the spontaneous decay rate of the state, and  $S$  is the source matrix for the state. As was discussed in GCH, the source matrix can represent either of the two closely related processes: population of the state by spontaneous decay of higher-lying excited states or direct optical excitation of the state by an external light beam.

When no rf field is present (when  $V=0$ ), the steady-state solution to (8) is<sup>6</sup>

$$\rho_{ij} = S_{ij} / (\Gamma + i\omega_{ij}). \quad (9)$$

We would like to determine how the solution (9) is modified when an rf field is applied to the atoms. Let us emphasize at the outset of our discussion that a full analysis of the effects of the

rf field is an exceedingly complex task, and a host of complicated phenomena are known to occur in intense rf fields. We intend to discuss in detail only the simplest situation in rf spectroscopy, a well-resolved single-quantum transition. This is the type of transition used in all of the measurements reported in this paper. We shall, however, briefly discuss certain multiple-quantum transitions which are observed in the  $P$  states, since these transitions serve to illustrate some peculiar properties of our cascade method of observation. We shall not attempt to analyze rf power shifts of the Bloch-Siegert-type<sup>13</sup> in any detail since our experimental conditions are always such that these shifts are negligibly small.

Suppose that the rf frequency  $\omega$  is nearly equal to the resonance frequency  $|\omega_{ij}|$  of a transition from the state  $i$  to the state  $j$ , that is,

$$\omega \approx (1/\hbar) |E_i - E_j| = |\omega_{ij}|. \quad (10)$$

Let us assume that the rf frequency is completely off-resonance for any other pair of levels  $r$  and  $s$ , i.e.,

$$|\omega - |\omega_{rs}|| \gg \Gamma \quad (11)$$

if  $(rs) \neq (ij)$ . Then the rf field will tend to equalize the population of the levels  $i$  and  $j$  without affecting the populations of any other sublevels. When the rf field is present, the steady-state density matrix  $\rho$  of (9) is replaced by the density matrix  $\rho'$

$$\rho' = \rho + \Delta\rho \quad (12)$$

where the increment  $\Delta\rho$  is caused by the rf field and is

$$\Delta\rho = -Pf + (\text{rf coherence}) + (\text{small higher-order and off-resonance terms}). \quad (13)$$

Here the initial relative polarization of the levels  $i$  and  $j$  is

$$P = (1/2\Gamma)(S_{ii} - S_{jj}) \times (|i\rangle\langle i| - |j\rangle\langle j|), \quad (14)$$

and the line-shape factor is<sup>10</sup>

$$f = \frac{\omega_1^2}{\Gamma^2 + \omega_1^2 + (\omega - \omega_{ij})^2}. \quad (15)$$

The nutational frequency  $\omega_1$  is

$$\omega_1 = \langle i|V|j\rangle / \hbar. \quad (16)$$

The small higher-order and off-resonance terms, which describe rf power shifts and other more complicated effects, are of no importance if the rf field is not too large, and we shall ignore them from now on. The rf coherence between the levels

$i$  and  $j$  can be quite large. However, we shall also ignore the rf coherence, since it causes a modulation of the fluorescent light at the rf frequency  $\omega$ , but it does not affect the average intensity of the fluorescent light. Since we observe the average value of the fluorescent light in our experiments, the rf coherence can have no effect on our measurements. Also, if the rf coherence is produced by an rf transition in a feeder state, rather than directly in the fluorescing state, it will ordinarily be strongly degraded by each step of cascading from the feeder state to the fluorescing state.

The static polarization  $P$  of (13) does affect the mean value of the fluorescent light, and it can also be carried with good efficiency from a feeder state to a fluorescing state. We shall therefore limit our attention to the influence of  $P$  on the fluorescent light.

### C. Transitions in the Fluorescing State

If an rf transition is induced in the fluorescing state, the expectation value of the electronic angular momentum will be

$$\langle J_z \rangle = \text{Tr}[\rho_b J_z] - f \text{Tr}[P J_z]. \quad (17)$$

The first term on the right of (17) is the decoupling signal which was discussed in GCH. The second term on the right of (17) is the rf resonance, and it contains the line-shape factor  $f$  of (15) and an amplitude  $\text{Tr}[P J_z]$ . We note that the rf transition will generate an observable signal only if the mean electronic spin  $\langle i | J_z | i \rangle$  differs from the mean electronic spin  $\langle j | J_z | j \rangle$  for the two sublevels  $i$  and  $j$  connected by the transition. Otherwise, the amplitude factor  $\text{Tr}[P J_z]$  will be zero. Both the decoupling background signal  $\text{Tr}[\rho_b J_z]$  and the amplitude factor  $\text{Tr}[P J_z]$  may vary slightly as the static magnetic field is swept through the resonance condition  $\omega = |\omega_{ij}|$ . This will cause the rf resonance to appear on a sloping base line, and this can lead to small shifts in the frequency of the peak of the experimental resonance curve from the true resonance frequency  $|\omega_{ij}|$ . In our experimental procedure we try to operate under conditions such that both  $\text{Tr}[\rho_b J_z]$  and  $\text{Tr}[P J_z]$  are nearly constant across the resonance line, and in analyzing the data we try to eliminate the frequency shifts due to the sloping base line.

As a simple example, we shall work out the theoretical amplitude for an rf transition in a fluorescing  $S$  state. In GCH it was shown that if the static magnetic field is not too small, the source matrix for an  $S$  state populated by spontaneous decay of a higher-lying, optically excited  $P$  state is

$$S = S_0 + S_1 s_z J_z, \quad (18)$$

where the constants  $S_0$  and  $S_1$  were listed in Table II of GCH, and  $s_z$  is the mean longitudinal spin of the photons used to excite the  $P$  state. From (12) we deduce that the mean value of  $J_z$  is

$$\langle J_z \rangle = (S_1 s_z / \Gamma)(2I + 1) \{y - \Delta y f\} + \dots, \quad (19)$$

where the line-shape factor  $f$  was defined in (15), and the quantity  $y$  was defined by Eq. (26) of GCH. For  $A\tau_b \gg 1$ , where  $A$  is the magnetic dipole coupling constant of the  $S$  state and  $\tau_b$  is the lifetime, we have

$$y \approx \frac{1}{2I + 1} \sum_k |\langle k | J_z | k \rangle|^2 \quad (20)$$

and also

$$\Delta y = \frac{1}{2I + 1} |\langle i | J_z | i \rangle - \langle j | J_z | j \rangle|^2. \quad (21)$$

Now both  $y$  and  $\Delta y$  have a simple interpretation in terms of the Breit-Rabi diagram of Fig. 2. The diagonal matrix element  $\langle i | J_z | i \rangle$  is the rate of change (in units of  $g_J \mu_B$ ) of the energy level  $E_i$  with magnetic field. Consequently, the decoupling signal  $y$  at a given magnetic field is the sum of the squares of the slopes of all of the energy levels in the Breit-Rabi diagram. It is evident that the decoupling signal  $y$  increases as the magnetic field increases, since the slopes of most of the energy levels become steeper at higher fields. The amplitude  $\Delta y$  of the rf signal also varies with the external field, since  $\Delta y$  is proportional to the square of the difference of the slopes of the initial and final levels. The quantities  $y$  and  $\Delta y$  are

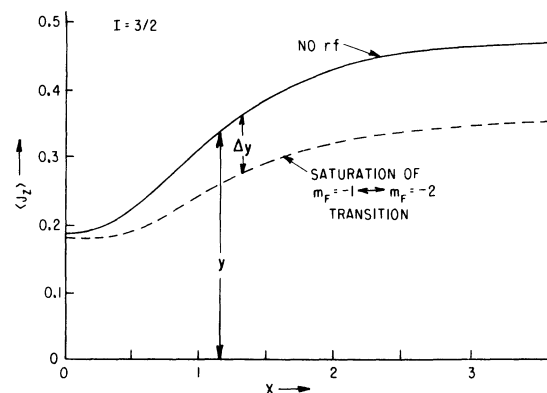


FIG. 3. Change in the electronic polarization (solid line) of a  $^2S_{1/2}$  state (nuclear spin  $I = \frac{3}{2}$ ) as a function of the external magnetic field [plotted in units of the Breit-Rabi parameter  $x = (g_J - g_I)\mu_B H / h\nu$ ]. The dotted line shows the electronic polarization as a function of  $x$  if the population of one pair of sublevels ( $m_F = -2$  and  $m_F = -1$ ) is equalized. The magnitude of the rf signal for saturation of the  $m_F = -2 \leftrightarrow -1$  transition,  $\Delta y$ , is proportional to the vertical distance between the two curves.

sketched in Fig. 3 for the transition ( $F=I+\frac{1}{2}$ ,  $m_F = -I+\frac{1}{2} \leftrightarrow F=I+\frac{1}{2}$ ,  $m_F = -I-\frac{1}{2}$ ). We note that the amplitude  $\Delta y$  of the rf signal increases by a factor of  $(2I+1)^2$  as the magnetic field at resonance increases from the completely coupled to the completely uncoupled regime. Consequently, it is very advantageous to take data in the high-field, uncoupled regime. Simple, explicit formulas for  $\Delta y$  can be derived from Eq. (21) and Eqs. (31) and (32) of GCH.

#### D. Transfer of Atomic Polarization by Cascading

If the atomic state  $b$  is produced by spontaneous decay of a higher state  $e$ , the source matrix  $S$  of the state  $b$  is

$$S_{ij}(b) = \sum_{rs} T_{ij,rs}(be) \rho_{rs}(e), \quad (22)$$

where the matrix  $T$  is [see Eq. (9) of GCH]

$$T_{ij,rs}(be) = \frac{4e^2\omega_{eb}}{3m^2c^3\hbar} \langle i|\vec{p}|r\rangle \cdot \langle s|\vec{p}|j\rangle. \quad (23)$$

It is convenient to write (22) in abbreviated matrix form

$$S(b) = T(be)\rho(e). \quad (24)$$

From (22) and (8) it follows that in the absence of an rf field the steady-state density matrix  $\rho(b)$  is

$$\rho_{ij}(b) = \sum_{rs} G_{ij,rs}(be) \rho_{rs}(e), \quad (25)$$

where

$$G_{ij,rs}(be) = T_{ij,rs}(be)/(\Gamma_b + i\omega_{ij}). \quad (26)$$

We shall also write (26) in abbreviated matrix form

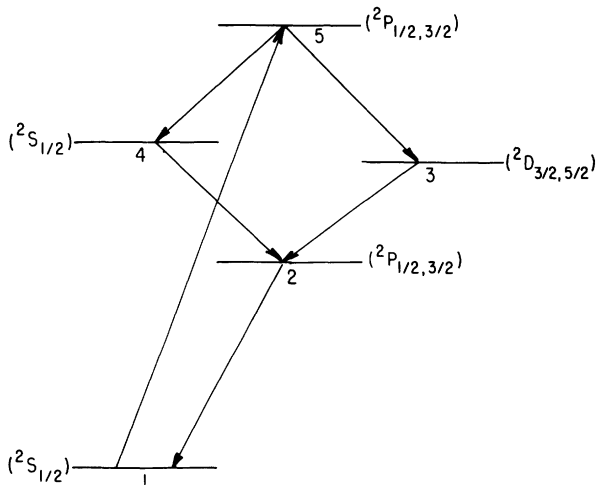


FIG. 4. Energy-level scheme of the various states involved in a typical cascade-fluorescence experiment.

$$\rho(b) = G(be)\rho(e). \quad (27)$$

For future reference we note that

$$\begin{aligned} G(be)\rho(e) &= \frac{1}{\Gamma_b} \{T(be)\rho(e)\}_{av} \\ &= \frac{1}{\Gamma_b} \int_0^\infty e^{-i\mathcal{H}_0 t} [T(be)\rho(e)] \\ &\quad \times e^{i\mathcal{H}_0 t - \Gamma_b t} \Gamma_b dt, \end{aligned} \quad (28)$$

where  $\mathcal{H}_0$  is the Hamiltonian operator of the state  $b$ .

We often deal with a situation in which a lower-lying state  $b$  is fed by a higher-lying state  $e$  through several different decay routes. For instance, in Fig. 4 the state 1 is fed by the state 5 by direct spontaneous decay and by two cascading routes, one through the state 4 and one through the state 3. Consequently, we shall define a general transfer matrix  $C(be)$  which relates the polarization of a higher-lying feeder state  $e$  to a lower-lying state  $b$ . We have

$$C(be) = \sum_{rs\dots t} G(br)G(rs)\dots G(te), \quad (29)$$

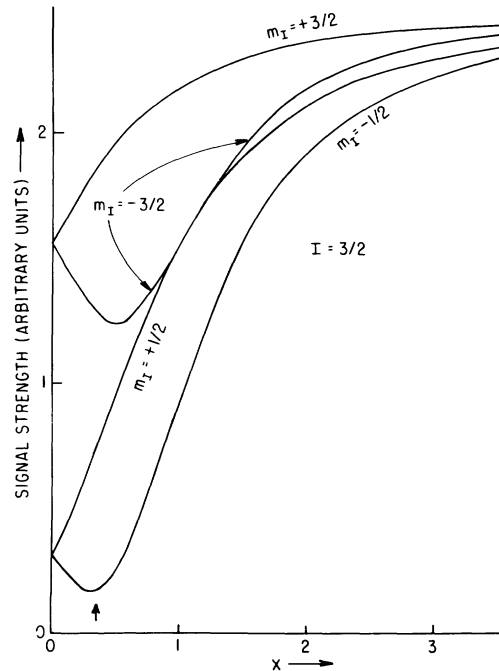


FIG. 5. Relative intensities of rf resonances in a  ${}^2P_{3/2}$  state as a function of the external magnetic field if the resonances are observed in cascade via a  ${}^2S_{1/2}$  state. The external magnetic field has been plotted in units of the Breit-Rabi parameter  $x = [(g_J - g_I)\mu_B H / h\Delta\nu]$  for the  ${}^2S_{1/2}$  state. The  ${}^2P_{3/2}$  state has been assumed to be completely decoupled. The vertical arrow indicates the field at which resonances in the  ${}^7P_{3/2}$  state of  $\text{Rb}^{87}$  were observed [see Fig. 8(b) and the text].

where the summation in (29) extends over all cascade routes from  $e$  to  $b$ . For instance, in the specific example sketched in Fig. 4,

$$C(15) = G(15) + G(12)G(24)G(45) + G(12)G(23)G(35). \quad (30)$$

#### E. rf Transitions in a Feeder State

Radio-frequency transitions in a feeder state  $e$  can also be readily observed, since the cascading will transfer the polarization change in the feeder state to the fluorescing state  $b$ . The mean value of the electronic angular momentum in the state  $b$  is

$$\langle J_z \rangle = \text{Tr}[\rho_b J_z] - f \text{Tr}[J_z C(be) P_e], \quad (31)$$

where  $f$  is the line-shape factor of (15),  $C(be)$  is the cascade transfer matrix discussed in Sec. II D, and  $P_e$  is the relative polarization [Eq. (14)] of the sublevels  $i$  and  $j$  of the feeder state  $e$ . Just as in the case of rf transitions in the fluorescing state, there is a decoupling background signal  $\text{Tr}[\rho_b J_z]$  and an rf amplitude  $\text{Tr}[J_z C(be) P]$ , both of which may vary slightly as the magnetic field is swept across the resonance line. Unless the electronic and nuclear spins are completely decoupled in all of the excited atomic states, the evaluation of the rf amplitude involves so much matrix algebra that it is best done with electronic computers. For narrow magnetic resonance lines, however, it is probably unnecessary to make detailed calculations of the decoupling signal and the rf amplitude, since the distortion of the resonance line caused by the variation of these quantities with the magnetic field can be accounted for by a least-squares analysis of the experimental data. We believe that the rf resonances in the  $5^2S_{1/2}$  states of  $K^{39}$  and  $K^{41}$ , the  $6^2S_{1/2}$  states of  $Rb^{85}$  and  $Rb^{87}$ , and the  $7^2S_{1/2}$  state of  $Cs^{133}$  are not significantly distorted, although all of these states feed the lowest  $P$  state of the atoms, and the rf transitions are detected by monitoring the changes induced in the fluorescence of the lowest  $P$  state.

Although we do not expect the intervening stages of cascading to have much effect on the apparent center frequency of a resonance in a feeder state, surprising modifications of the rf amplitude can occur. For instance, in Fig. 8(b) one can see that the four rf transitions corresponding to the four different values of  $m_I$  in the  $7^2P_{3/2}$  state of  $Rb^{87}$  have strikingly different amplitudes. This particular situation is amenable to simple theoretical analysis, and we shall discuss it in some detail here, since it gives some insight into the mechanisms of cascade fluorescence spectroscopy.

Let us assume that the external magnetic field is large enough to decouple  $I$  and  $J$  in the  $7^2P_{3/2}$

state. Then the eigenstates of the atom are very nearly  $|m_I m_J\rangle$ , where  $m_I$  and  $m_J$  are the nuclear and electronic azimuthal quantum numbers. The density matrix of an optically excited  $7^2P_{3/2}$  state is

$$\rho_e = \sum_{L=0}^2 B_L T_{L0}(J_e J_e) \sum_{m_I} |m_I\rangle \langle m_I|, \quad (32)$$

where the coefficients  $B_L$  of (32) can be obtained from Eq. (20) of GCH. Let us further suppose that the electric quadrupole coupling constant  $B$  is negligibly small compared to the nutational frequency  $\omega_1$ :

$$B \ll \omega_1 = g_J (\mu_B / 2\hbar) H_1. \quad (33)$$

Then an rf field of the frequency

$$\omega_\mu = (1/\hbar) g_J \mu_B H + 2\pi A \mu \quad (34)$$

can couple the states  $|\mu J\rangle, |\mu, J-1\rangle, \dots, |\mu, -J\rangle$ , and this set of sublevels will undergo magnetic resonance as if it were an isolated, evenly spaced Zeeman multiplet. Consequently, if magnetic resonance is induced by a radio-frequency field of frequency  $\omega \approx \omega_\mu$ , the density matrix of the  $P_{3/2}$  state will become

$$\rho'_e = \rho_e - \sum_{L=1}^2 P_L f_L + (\text{rf coherence}) + \dots \quad (35)$$

The multipole polarizations are

$$P_L = B_L T_{L0}(J_e J_e) |\mu\rangle \langle \mu|, \quad (36)$$

and the multipole line-shape functions are of the Bloch form

$$f_1 = \frac{\omega_1^2}{\omega_1^2 + \Gamma^2 + (\omega - \omega_\mu)^2} \quad (37)$$

and the Brossel-Bitter form<sup>1</sup>

$$f_2 = \frac{3\omega_1^2 [\Gamma^2 + \omega_1^2 + 4(\omega - \omega_\mu)^2]}{[\Gamma^2 + 4\omega_1^2 + 4(\omega - \omega_\mu)^2][\Gamma^2 + \omega_1^2 + (\omega - \omega_\mu)^2]}. \quad (38)$$

Now from Eq. (10) of GCH, we find that

$$T(be) P_L = \Gamma_{eb} |\mu\rangle \langle \mu| (2J_e + 1) W(1J_e J_b L; J_b J_e) \times B_L T_L(J_b J_b). \quad (39)$$

Since the state  $b$  is a  $2S_{1/2}$  state, the alignment (the term with  $L=2$ ) is lost when the atom cascades from  $e$  to  $b$ . This can be seen formally by noting that the triangle condition on the arguments  $(J_b J_b L)$  of the Racah coefficient cannot be satisfied when  $J_b = \frac{1}{2}$  and  $L=2$ . Consequently, the polarization induced in the  $2S_{1/2}$  state by an rf transition between the sublevels  $|\mu J\rangle, |\mu, J-1\rangle, \dots, |\mu, -J\rangle$  is [see (28)]

$$C(be) P_1 \propto \{J_z |\mu\rangle \langle \mu|\}_{av} \quad (40)$$

where we have set  $T_{10}(J_a J_b) = J_z \sqrt{2}$ . The amplitude of the rf resonance is therefore proportional to

$$y_\mu = \frac{1}{2I+1} \text{Tr}[J_z \{J_z | \mu \rangle \langle \mu | \}_{J_{av}}]. \quad (41)$$

We note that the decoupling signal from the S state is

$$y = \sum_\mu y_\mu, \quad (42)$$

where a simplified expression for  $y$  was given by Eq. (20). The quantity  $y_\mu$  can be evaluated explicitly with the formulas of Sec. II F of GCH. We find for  $A\tau_b \gg 1$  in the S state,

$$y_\mu \approx \frac{1}{4(2I+1)} \sum_{m=\mu-1/2}^{\mu+1/2} \frac{z^2}{v^2+z^2} \quad (43)$$

where the quantities  $z$  and  $v$  depend on  $m$  and are

$$v^2 = (I + \frac{1}{2})^2 - m^2, \quad (44)$$

$$z = m + x(I + \frac{1}{2}). \quad (45)$$

The field parameter for the Breit-Rabi formula is

$$x = \frac{\mu_B H (g_J - g_I)}{hA(I + \frac{1}{2})}. \quad (46)$$

Now Eq. (43) also has a simple graphical interpretation in terms of the Breit-Rabi diagram of Fig. 2. The slope (rate of change of energy with respect to magnetic field, in units of  $g_J \mu_B$ ) of an energy level which evolves from the upper Zeeman multiplet is  $z/2(z^2 + v^2)^{1/2}$ . Consequently, the amplitude of an rf transition which equalizes the populations of the sublevels with  $m_I = \mu$  in the  $P_{3/2}$

state is proportional to the sum of the squares of the slopes of the levels with  $m = \mu - \frac{1}{2}$  and  $m = \mu + \frac{1}{2}$  in the upper Zeeman multiplet of the  $S_{1/2}$  state. As an example, the theoretical rf amplitudes for an atom with  $I = \frac{3}{2}$  are plotted in Fig. 5. The observed amplitudes of Fig. 8 are in good agreement with the predicted amplitudes of Fig. 5. We note that for high fields the theoretical amplitudes all approach the same limiting value, which is  $(2I+1)$  times smaller than the decoupling signal.

In summary, because of the recoupling of  $I$  and  $J$ , intervening stages of cascading can profoundly alter the amplitude of an rf transition in a high-lying feeder state.

### III. APPARATUS

The details of our experimental arrangement are shown in Fig. 6. The appropriate resonance lines from an alkali-metal-vapor lamp are selected by an interference filter. For example, to investigate the  $7^2S_{1/2}$  state of Rb, we select the 3587-Å and 3592-Å ( $7^2P_{3/2,1/2} - 5^2S_{1/2}$ ) lines. The interference-filter bandwidth is typically about 100 Å; i.e., we make no attempt to filter out one of the two fine-structure components. The resonance lines then pass through a Polaroid HNP'B linear polarizer, a mica quarter-wave plate, and are incident on a Pyrex cell containing alkali metal. The cell is placed inside a coaxial transmission line near its shorted end in such a way that the rf magnetic field is perpendicular to the static magnetic field. This arrangement ensures that the cell is in the maximum rf magnetic field and helps prevent the

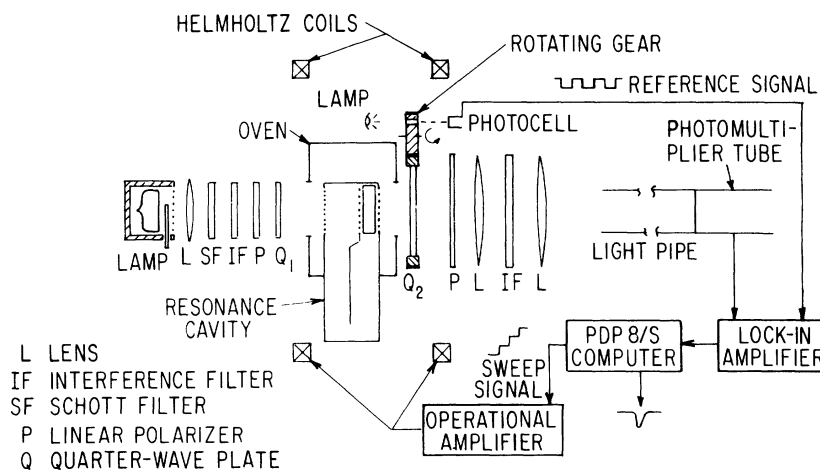


FIG. 6. Details of our experimental arrangement. The appropriate resonance lines from an alkali-metal-vapor lamp are selected by an interference filter, circularly polarized, and are incident on a Pyrex cell containing alkali metal. This cell is placed inside a rf cavity, and a longitudinal static magnetic field is maintained at the cell by a pair of Helmholtz coils. The appropriate fluorescent light is selected by an interference filter, analyzed for circular polarization, and detected by a photomultiplier tube. Lock-in techniques are used, and a PDP-8/S computer is used for signal averaging.



problem of discharge in the cell. The details of the transmission line, which we shall refer to as "cavity," will be described below. The static magnetic field is maintained along the axis of the apparatus by a pair of Helmholtz coils. The cavity is also used as an oven so that sufficient vapor pressure of the alkali metal can be obtained. The fluorescent light passes through a Polaroid quarter-wave plate, a linear polarizer, and is frequency selected by the interference filter. The light is detected by a dry-ice-cooled extended-red-response S-20 photomultiplier tube.

We use a Schott colored glass filter directly in front of the lamp to further suppress the direct leakage of light from the lamp to the photomultiplier tube. The Schott filters that we have used have a high transmission for the exciting-light wavelengths but also have a very high attenuation at the fluorescent-light wavelength region (near ir). In order to have a large solid angle of detection, we use a large (4×4 in.) interference filter in the detection stage. Since the peak transmission of an interference filter shifts for oblique incidence, we have sandwiched the interference filter between two large Fresnel lenses in such a way that the light incident on the interference filter is more or less parallel. We use lock-in techniques to detect the polarization of the fluorescent light. The quarter-wave plate  $Q_2$  is mounted on a gear which is rotated at  $6\frac{1}{2}$  revolutions per second by a synchronous motor. The light reaching the photomultiplier tube is thus modulated at 13 Hz, the degree of modulation being proportional to the degree of circular polarization of the fluorescent light. A reference signal at 13 Hz is also generated by the rotating gear, and the intensity of the polarized fluorescent light is detected by a phase-sensitive detector. The rf resonance signal is usually quite small, so further signal averaging is performed with the aid of a PDP-8/S computer.

*Lamp.* Two different types of lamps were used in these investigations. One type consisted of a 2-in.-diam. Pyrex bulb with a flat window placed inside a microwave cavity. The bulb contained separated isotope of the alkali metal and about 0.1 to 0.5 torr of buffer gas, usually Kr. The cavity was heated with cartridge heaters to obtain sufficient alkali-metal vapor pressure. A commercial diathermy unit (about 60–70 W output at 2450 MHz) was used to excite the discharge in the lamp. The bulb was placed in the cavity in such a way that the most intense discharge in the bulb was near its front window, thus minimizing the problem of self-reversal of the resonance lines.

The second kind of lamp consisted of a 1-in.-diam. and about 3-in.-long bulb placed inside the tank circuit coil of a ~30 MHz oscillator. The coil

was placed inside an oven. This bulb contained alkali metal, and no buffer gas was used. The bulbs were made of Pyrex for Rb and Cs and of an alkali-resistant Osram glass for K. The two types of lamp were used with about equal success.

*Resonance Cavity and the Cell.* The rf magnetic field at the cell should be sufficiently large to ensure that there is a good probability of inducing magnetic dipole transitions between the magnetic sublevels of the atom within the lifetime of the state. Lifetimes of the states that we have investigated are typically of the order of 100 nsec, and a rf magnetic field of about 1–2 G is required in order to see a good signal. Such fields are conveniently obtained by placing the cell near the shorted end of a coaxial transmission line. Near the shorted end, the rf magnetic field is maximum, while the rf electric field is minimum. This helps prevent a discharge from occurring inside the cell. The details of our cavity, which was constructed to resonate around 147 MHz, are shown in Fig. 7. The cavity was made from a 3×4×23 in. aluminum box with a removable cover plate. A center conductor, made of a 2½-in.-wide copper strip, was mounted with one end firmly in contact with the wall of the cavity and the other supported on a ceramic insulator. The center conductor was bent toward the cell, as shown in the figure, in order to maximize the rf magnetic field at the cell. The length of the central conductor is about a quarter of a wavelength. The resonance frequency of the cavity was measured with a grid-dip meter, and the length of the conductor was varied until the box resonated at the desired frequency. A small tuning capacitor, made of a flat disc mounted at the end of a screw, was used to tune the cavity in the neighborhood of 147 MHz.

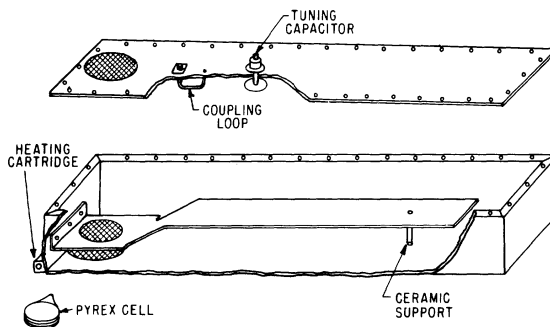


FIG. 7. Details of our radio-frequency "cavity." The cavity consists of a coaxial transmission line, quarter wavelength long and shorted at the left end. The alkali-metal-vapor cell is placed near the shorted end of the cavity. The rf magnetic field is a maximum at the shorted end, while the rf electric field is a minimum. The cell has internal partitions to eliminate multipactor breakdown of the alkali-metal vapor.

The exciting light and the fluorescent light could pass through screens mounted on the walls and on the central conductor of the cavity. Two cartridge heaters were mounted on the cavity walls so that the cell could be heated until the desired vapor pressure of the alkali metal was obtained. Part of the heating was done by the rf itself. As a matter of fact, rf heating of the cell was a good indication of the rf power absorption in the cavity. For this reason, we continuously monitored the temperature of the cell with a thermocouple during the run. A similar cavity was constructed for use at 405 MHz. This cavity is almost identical to the 147-MHz cavity except that the central conductor is a half wavelength long, and the shorted end is at the center of the cavity. The 147-MHz cavity was driven by a 2-m-band amateur radio transmitter and the 405-MHz cavity by a Bird Electronics cavity oscillator.

Although our cavity arrangement helps in preventing the problem of discharge in the cell, during our initial efforts we found that discharge remained a problem at high rf fields. We now believe that the breakdown in the cell was caused, at least in part, by multipactor effect.<sup>14</sup> Consider an electron which is accelerated by the rf electric field and strikes a wall (wall A) of the cell, emitting secondary electrons. If during this time the rf electric field has reversed, the secondary electrons will find themselves in the right phase to be accelerated toward the opposite wall (wall B). If the transit time of these electrons across the cell is an odd integral multiple of one-half cycle of the rf field, these electrons will become the primary electrons at wall B, and the secondary electrons emitted there will be accelerated back toward wall A. If the secondary-electron emission ratio of the cell wall is greater than 1, the effect can lead to a buildup of large electron densities in the cell. This causes an eventual breakdown of the vapor. An analysis of the effect shows<sup>14</sup> that for a given frequency of rf field, there exists a cutoff gap length. If the gap is smaller than this length, the right phase conditions for the electrons cannot be satisfied, and multipactor breakdown cannot occur. At 147 MHz, this gap separation is about 5 mm. Therefore, we have made our cells with a gap of about 3 mm. However, by making the cell thin, we lose in the amount of fluorescent light that we can get, as the vapor density of the alkali metal cannot be increased arbitrarily due to collisional depolarization in the excited states.<sup>6</sup> We have, therefore, made our cells with several internal partitions. Each section of the cell has a 3-mm gap between opposite walls.

*Signal Averaging.* A PDP-8/S computer was

used for data accumulation. The region of magnetic field where the resonance was expected was divided into a number of "channels," usually 64. The computer was programmed to generate a sweep voltage consisting of 64 steps. This voltage was used to drive an operational amplifier which supplied current to the Helmholtz coils. At each "step" of the magnetic field, the computer sampled the output of the lock-in amplifier, digitalized it, and stored it in a particular memory location. Thus, there were 64 memory locations, each corresponding to a given value of the magnetic field. In this fashion, the magnetic field was swept through the region of interest in 64 discrete steps, and at each step of the magnetic field, the output of the lock-in amplifier was stored in the computer memory. This operation was performed repeatedly until a signal was observed with the desired signal-to-noise ratio. In this way, large signal-averaging times were achieved, and several of our runs lasted 8 to 10 hours. The data stored in the computer memory could be displayed on an oscilloscope screen for inspection and could be read out on a teletype.

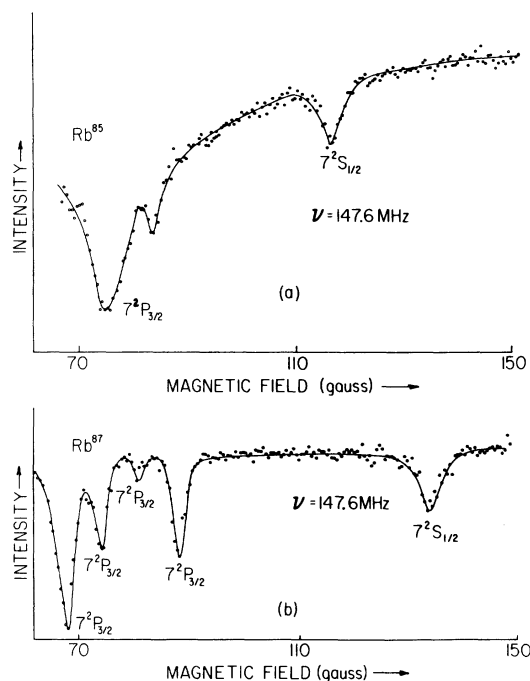


FIG. 8. Experimental curves with resonances in the  $7^2S_{1/2}$  state of  $\text{Rb}^{85}$  (a) and of  $\text{Rb}^{87}$  (b). The  $\text{Rb}^{85}$  resonance curve is due to the  $m_F = -3 \leftrightarrow m_F = -2$ ,  $\Delta F = 0$  transition, while the  $\text{Rb}^{87}$  resonance is due to the  $m_F = -2 \leftrightarrow m_F = -1$ ,  $\Delta F = 0$  transition. The transition frequency in both cases is 147.6 MHz. The rf resonances in the  $7^2P_{3/2}$  state are also observed (shown at the left) in the  $7408\text{-}\text{\AA}$  ( $7^2S_{1/2} \rightarrow 5^2P_{3/2}$ ) observation channel, since the  $7^2S_{1/2}$  state is populated via the  $7^2P_{3/2}$  state.

## IV. RESULTS

Examples of the curves obtained in our rf resonance measurements are given in Figs. 8–13. The radio-frequency resonance curve in the  $7^2S_{1/2}$  state of  $\text{Rb}^{85}$  at about 116 G is shown in Fig. 8(a). This resonance is due to transitions between sub-levels with quantum numbers  $F=3, m_F=-3$  and  $F=3, m_F=-2$ , at 147 MHz. The corresponding resonance in the  $7^2S_{1/2}$  state of  $\text{Rb}^{87}$  is shown in Fig. 8(b). These resonances were observed in the 7408-Å ( $7^2S_{1/2}-5^2P_{3/2}$ ) fluorescent light. The temperature of the cell was around 150°C. We were not able to go higher in temperature, as the collisional depolarization in the excited states degrades the signal significantly at higher temperatures. Of course, at lower temperatures there is much less fluorescence. A more detailed description of the effects of collisional depolarization in the excited states has been given in connection with decoupling spectroscopy.<sup>6</sup> We try to collect the data at such cell temperatures that the signal-to-noise ratio is optimum. The resonance signal was approximately 12% of the polarization of the fluorescent light.

Since the  $7^2S_{1/2}$  state is populated via the  $7^2P$  states, any rf transitions in the  $7^2P$  states will affect the polarization of the  $7^2S_{1/2}$  state and will, consequently, be observable in the 7408-Å (or 7280-Å) fluorescent light. Indeed, we see four well-resolved resonances in the  $7^2P_{3/2}$  state of  $\text{Rb}^{87}$  in the vicinity of 80 G. For the  $7^2P_{3/2}$  state, 80 G is a sufficiently high magnetic field so that  $m_I$  and  $m_J$  are good quantum numbers. Each of the four well-resolved resonances in  $\text{Rb}^{87}$  is due to three unresolved transitions,  $m_J = +\frac{3}{2} \rightarrow +\frac{1}{2}$ ,  $m_J = +\frac{1}{2} \rightarrow -\frac{1}{2}$ , and  $m_J = -\frac{1}{2} \rightarrow -\frac{3}{2}$  for a given value of  $m_I$ . For  $\text{Rb}^{87}$ , the nuclear spin  $I$  has a value

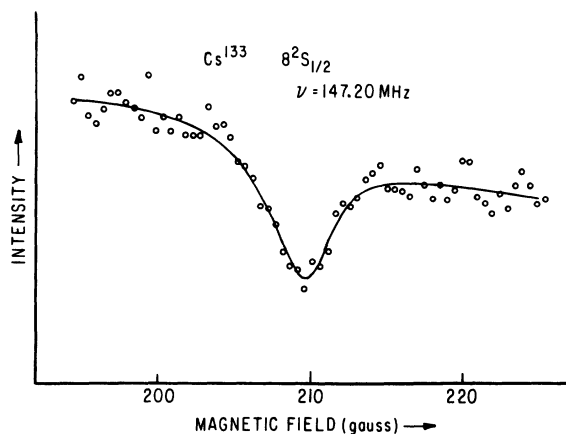


FIG. 9. rf resonance curve due to the  $m_F = -4 \rightarrow m_F = -3$ ,  $\Delta F = 0$  transition in the  $8^2S_{1/2}$  state of  $\text{Cs}^{133}$ . Total integration time was about 3 h.

of  $\frac{3}{2}$ ; therefore, four resonances correspond to four different values of  $m_I$ . In  $\text{Rb}^{85}$  ( $I = \frac{5}{2}$ ) the six resonances are not well resolved.

As it was pointed out in Sec. II E, the intensities of various resonance can get modified in the cascading process due to the recoupling of electronic and nuclear angular momenta in the intervening stages. In Fig. 8(b), the four  $7^2P_{3/2}$  resonances are seen to have curious intensity ratios. If these resonances were observed in 3587-Å resonance fluorescence, they would have equal intensity, since this is the Paschen-Back region for the  $7^2P_{3/2}$  state. However, the observed signal, i.e., the depolarization of the  $7^2S_{1/2}-5^2P_{3/2}$  (7408-Å) fluorescent light, is proportional to the change in the *electronic* polarization of the  $7^2S_{1/2}$  state when a magnetic dipole transition among the sub-levels of the  $7^2P_{3/2}$  state is induced. The hfs of the  $7^2S_{1/2}$  state is much larger ( $A = 318$  MHz) than the hfs of the  $7^2P_{3/2}$  state, and, therefore, the nuclear angular momentum is strongly coupled to the electronic angular momentum in the  $7^2S_{1/2}$  state at 80 G field. The coupling of the nuclear spin affects the electronic polarization of the  $7^2S_{1/2}$  state, which gives rise to different signal strengths for different resonances. A quantitative treatment of this effect was given in Sec. II E. A similar intensity distribution among various resonances exists in the case of  $\text{Rb}^{85}$ . The resonance

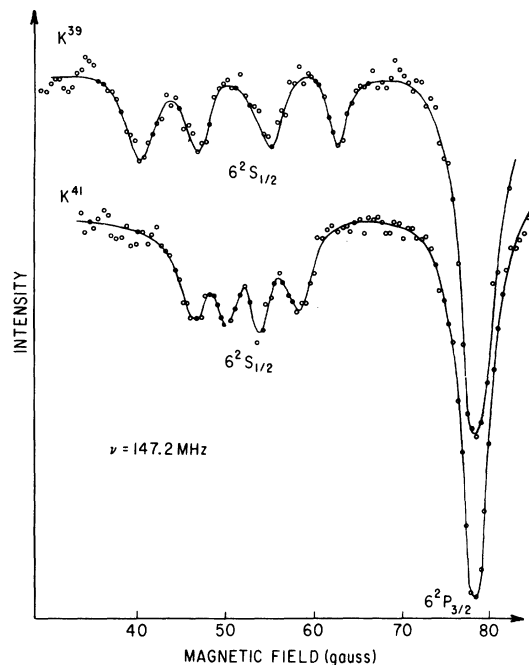


FIG. 10. rf resonances in the  $6^2S_{1/2}$  states of  $\text{K}^{39}$  and  $\text{K}^{41}$ . The sharp decrease in the intensity of the polarized light around 79 G is due to unresolved transitions in the  $6^2P_{3/2}$  state.

TABLE I. A list of relevant parameters for all the states that have been investigated in this work.

| Element           | State                           | Exciting light  | Observed fluorescent light  | Schott filter(s) used          | Approximate temperature of the cell (°C) | Theoretical lifetime of the state (nsec) | Approximate transition frequency (MHz) | Observed transition(s)   | Magnetic field at which resonance observed (G) | Signal strength (%) |
|-------------------|---------------------------------|---|---|--------------------------------|--|--|--|--|--|---------------------|
| K <sup>39</sup>   | 5 <sup>2</sup> S <sub>1/2</sub> | 5 <sup>2</sup> P <sub>1/2,3/2</sub> → 4 <sup>2</sup> S <sub>1/2</sub><br>4045 Å<br>4047 Å | 4 <sup>2</sup> P <sub>3/2</sub> → 4 <sup>2</sup> S <sub>1/2</sub><br>7645 Å | BG38(2 mm)                     | 80 <sup>a</sup>                          | 46.7 <sup>b</sup>                        | 404.8                                  | m <sub>J</sub> = - $\frac{3}{2}$ ↔ + $\frac{1}{2}$   | 172.3  | 3.5                 |
|                   |                                 | 6 <sup>2</sup> P <sub>1/2,3/2</sub> → 4 <sup>2</sup> S <sub>1/2</sub><br>3447 Å<br>3448 Å | 6 <sup>2</sup> S <sub>1/2</sub> → 4 <sup>2</sup> P <sub>1/2</sub><br>6911 Å | UG1(2 mm)                      | 185                                      | 90.9 <sup>b</sup>                        | 147.1                                  | m <sub>J</sub> = - $\frac{3}{2}$<br>m <sub>J</sub> = + $\frac{3}{2}$<br>m <sub>J</sub> = - $\frac{1}{2}$ ↔ + $\frac{1}{2}$ | 63.2<br>39.8                                   | 20                  |
| K <sup>41</sup>   | 5 <sup>2</sup> S <sub>1/2</sub> | 5 <sup>2</sup> P <sub>1/2,3/2</sub> → 4 <sup>2</sup> S <sub>1/2</sub><br>4045 Å<br>4047 Å | 4 <sup>2</sup> P <sub>3/2</sub> → 4 <sup>2</sup> S <sub>1/2</sub><br>7645 Å | BG38(2 mm)                     | 80 <sup>a</sup>                          | 46.7 <sup>b</sup>                        | 404.8                                  | m <sub>J</sub> = - $\frac{3}{2}$ ↔ + $\frac{1}{2}$   | 160.3  | 4                   |
|                   |                                 | 6 <sup>2</sup> P <sub>1/2,3/2</sub> → 4 <sup>2</sup> S <sub>1/2</sub><br>3447 Å<br>3448 Å | 6 <sup>2</sup> S <sub>1/2</sub> → 4 <sup>2</sup> P <sub>1/2</sub><br>6911 Å | UG1(2 mm)                      | 185                                      | 90.9 <sup>b</sup>                        | 147.4                                  | m <sub>J</sub> = - $\frac{3}{2}$<br>m <sub>J</sub> = + $\frac{3}{2}$<br>m <sub>J</sub> = - $\frac{1}{2}$ ↔ + $\frac{1}{2}$ | 58.5<br>45.9                                   | 20                  |
| Rb <sup>85</sup>  | 6 <sup>2</sup> S <sub>1/2</sub> | 6 <sup>2</sup> P <sub>1/2,3/2</sub> → 5 <sup>2</sup> S <sub>1/2</sub><br>4202 Å<br>4216 Å | 5 <sup>2</sup> P <sub>3/2</sub> → 5 <sup>2</sup> S <sub>1/2</sub><br>7800 Å | BG38(2 mm)                     | 60 <sup>a</sup>                          | 51.3 <sup>b</sup>                        | 405.0                                  | F = 3<br>m <sub>F</sub> = -2 ↔ -3  | 309.3  | 2.5                 |
|                   |                                 | 7 <sup>2</sup> P <sub>1/2,3/2</sub> → 5 <sup>2</sup> S <sub>1/2</sub><br>3587 Å<br>3592 Å | 7 <sup>2</sup> S <sub>1/2</sub> → 5 <sup>2</sup> P <sub>3/2</sub><br>7408 Å | BG18(1 mm)                     | 150                                      | 99.0 <sup>b</sup>                        | 146.9 <sup>c</sup>                     | F = 3<br>m <sub>F</sub> = -2 ↔ -3  | 115.9  | 12                  |
| Rb <sup>85</sup>  | 8 <sup>2</sup> S <sub>1/2</sub> | 8 <sup>2</sup> P <sub>1/2,3/2</sub> → 5 <sup>2</sup> S <sub>1/2</sub><br>3349 Å<br>3351 Å | 8 <sup>2</sup> S <sub>1/2</sub> → 5 <sup>2</sup> P <sub>1/2</sub><br>6071 Å | UG1(1 mm)<br>and<br>BG38(1 mm) | 140                                      | 188 <sup>c</sup>                         | 147.0                                  | F = 3<br>m <sub>F</sub> = -2 ↔ -3  | 87.5   | ~10                 |
|                   |                                 | 6 <sup>2</sup> P <sub>1/2,3/2</sub> → 5 <sup>2</sup> S <sub>1/2</sub><br>4202 Å<br>4216 Å | 5 <sup>2</sup> P <sub>3/2</sub> → 5 <sup>2</sup> S <sub>1/2</sub><br>7800 Å | BG38(2 mm)                     | 60 <sup>a</sup>                          | 51.3 <sup>b</sup>                        | 404.9                                  | F = 2<br>m <sub>F</sub> = -1 ↔ -2  | 361.2  | 2                   |
| Rb <sup>87</sup>  | 7 <sup>2</sup> S <sub>1/2</sub> | 7 <sup>2</sup> P <sub>1/2,3/2</sub> → 5 <sup>2</sup> S <sub>1/2</sub><br>3587 Å<br>3592 Å | 7 <sup>2</sup> S <sub>1/2</sub> → 5 <sup>2</sup> P <sub>3/2</sub><br>7408 Å | BG18(1 mm)                     | 150                                      | 99.0 <sup>b</sup>                        | 147.0                                  | F = 2<br>m <sub>F</sub> = -1 ↔ -2  | 134.3  | 10                  |
|                   |                                 | 8 <sup>2</sup> P <sub>1/2,3/2</sub> → 5 <sup>2</sup> S <sub>1/2</sub><br>3349 Å<br>3351 Å | 8 <sup>2</sup> S <sub>1/2</sub> → 5 <sup>2</sup> P <sub>1/2</sub><br>6071 Å | UG1(1 mm)<br>and<br>BG38(1 mm) | 140                                      | 188 <sup>c</sup>                         | 147.0                                  | F = 2<br>m <sub>F</sub> = -1 ↔ -2  | 107.5  | ~10                 |
| Cs <sup>133</sup> | 7 <sup>2</sup> S <sub>1/2</sub> | 7 <sup>2</sup> P <sub>1/2,3/2</sub> → 6 <sup>2</sup> S <sub>1/2</sub><br>4555 Å<br>4593 Å | 6 <sup>2</sup> P <sub>3/2</sub> → 6 <sup>2</sup> S <sub>1/2</sub><br>8621 Å | BG38(2 mm)                     | 30 <sup>a</sup>                          | 56.8 <sup>b</sup>                        | 404.8                                  | F = 4<br>m <sub>F</sub> = -3 ↔ -4  | 552.0  | 1.5                 |
|                   |                                 | 8 <sup>2</sup> P <sub>1/2,3/2</sub> → 6 <sup>2</sup> S <sub>1/2</sub><br>3876 Å<br>3888 Å | 8 <sup>2</sup> S <sub>1/2</sub> → 6 <sup>2</sup> P <sub>1/2</sub><br>7609 Å | BG18(1 mm)                     | 145                                      | 104 <sup>b</sup>                         | 147.0                                  | F = 4<br>m <sub>F</sub> = -3 ↔ -4  | 209.4  | 6                   |
| Cs <sup>133</sup> | 9 <sup>2</sup> S <sub>1/2</sub> | 9 <sup>2</sup> P <sub>1/2,3/2</sub> → 6 <sup>2</sup> S <sub>1/2</sub><br>3611 Å<br>3617 Å | 9 <sup>2</sup> S <sub>1/2</sub> → 6 <sup>2</sup> P <sub>1/2</sub><br>6355 Å | UG1(1 mm)<br>and<br>BG38(2 mm) | 105                                      | 192 <sup>c</sup>                         | 147.0                                  | F = 4<br>m <sub>F</sub> = -3 ↔ -4  | 152.7  | ~10                 |

<sup>a</sup> Estimated temperature.<sup>b</sup> O. S. Heavens, J. Opt. Soc. Am. 51, 1058 (1961).<sup>c</sup> P. Tsekeris (private communication).

corresponding to  $m_I = -\frac{5}{2}$  is seen to be clearly resolved from the other resonances owing to the fact that its two adjacent resonances ( $m_I = -\frac{3}{2}$  and  $m_I = -\frac{1}{2}$ ) have very small intensity. It is interesting to note that this effect may be used to advantage in those cases where the hfs is normally unresolved.

We should also observe resonances due to rf transitions among the magnetic sublevels of the  $7^2P_{1/2}$  state. Although several of these transitions lie in the magnetic field range of the curves shown in Fig. 8, these resonances are too weak to be observable. There are at least three different reasons for this. First, the oscillator strength ratios of the higher  $D$  lines in heavy alkalis are anomalous.<sup>15,16</sup> The  $5^2S_{1/2} \rightarrow 7^2P_{1/2}$  transition oscillator strength is several times weaker than the  $5^2S_{1/2} \rightarrow 7^2P_{3/2}$  oscillator strength. Second, the  $3592\text{-}\text{\AA}$  ( $7^2P_{1/2} \rightarrow 5^2S_{1/2}$ ) light from our lamp is several times weaker than the  $3587\text{-}\text{\AA}$  ( $7^2P_{3/2} \rightarrow 5^2S_{1/2}$ ) light. And finally, cascading through the  $7^2P_{1/2}$  state produces smaller electronic polarization in the  $7^2S_{1/2}$  state than does cascading through the  $7^2P_{3/2}$  state.<sup>6</sup>

In Figs. 9 and 10 we show resonances due to rf transitions in the second excited  $S$  states of  $\text{Cs}^{133}$  and  $\text{K}$ , respectively. The hfs intervals in both the isotopes of  $\text{K}$  are very small due to small values of the nuclear magnetic moments. We therefore see the unresolved  $6^2P_{3/2}$  resonances at the center of gravity for a  $2^2P_{3/2}$  state and all four rf resonances in the  $6^2S_{1/2}$  state. The  $\text{K}^{39}$  resonances are not quite in the Paschen-Back region and, therefore, are not symmetric about their center

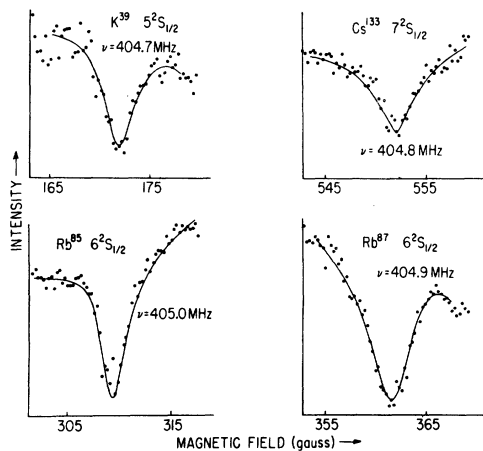


FIG. 11. rf resonance curves for the first excited  $S$  states of  $\text{K}^{39}$ ,  $\text{Cs}^{133}$ ,  $\text{Rb}^{85}$ , and  $\text{Rb}^{87}$ . The  $\text{Cs}^{133}$  resonance is due to the  $F=4$ ,  $m_F=-4 \rightarrow -3$  transition and the  $\text{Rb}^{85}$  curve is due to the  $F=3$ ,  $m_F=-3 \rightarrow -2$  transition, while both the  $\text{K}^{39}$  and  $\text{Rb}^{87}$  resonance curves are due to  $F=2$ ,  $m_F=-2 \rightarrow -1$  transitions.

of gravity. All relevant parameters for these and other resonances that we have observed (e.g., the wavelengths of the exciting and fluorescent lights, temperature of the alkali-metal cell, signal strengths, frequency, magnetic fields, and quantum numbers of the observed transitions) are listed in Table I. The values of signal strengths listed in Table I are the percentage change in the degree of polarization of the fluorescent light at the peak of the resonance. For example, in the case of the  $6^2S_{1/2}$  state of potassium, the polarization of the fluorescent light changes by 20% at each resonance. As there are four resonances, the rf transitions are about 80% saturated. We must emphasize that the values given in Table I for parameters such as signal strengths and cell temperatures are only representative values intended to give an idea of the general range of these parameters. Moreover, the frequency of transitions and the values for the magnetic field at which they occur vary somewhat from run to run, and the values listed in Table I are typical values. Note that only those resonances which are actually used to deduce the hfs values are listed in the table. For example, in the  $5^2S_{1/2}$  state of  $\text{K}^{41}$ , all four resonances have been observed, but extensive data have been taken only for the resonance at 160 G.

Data for the first excited  $S$  states are shown in Figs. 11 and 12. As pointed out in Sec. I, these resonances were observed in a two-step cascade, as the wavelength of the fluorescent light emitted during the first step in the cascading process lies well within the infrared region of the spectrum and cannot be detected by photomultiplier tubes. In all cases we have observed the  $D_2$  fluorescence. It will be noted from Table I that these data were taken with cell temperature much lower than for

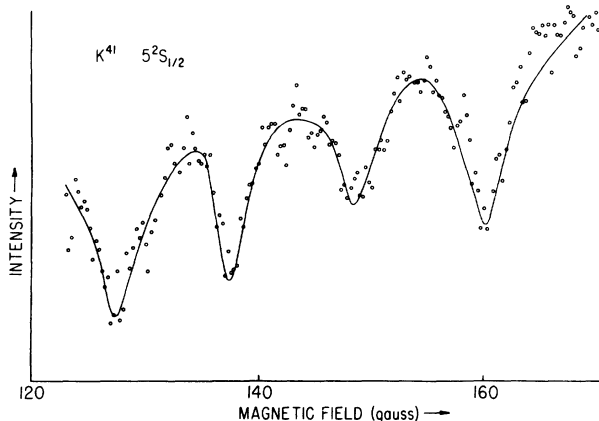


FIG. 12. rf resonances in the  $5^2S_{1/2}$  state of  $\text{K}^{41}$  for 404.8 MHz transition frequency.

the second excited S states. This was necessary in order to avoid depolarization of the fluorescent  $D_2$  light due to multiple scattering of the light in the cell. Therefore, in this case the temperature limitation was imposed by the multiple scattering of the  $D_2$  light rather than by collisional depolarization in the excited states. Good signals were, however, obtained, since the second-resonance lines were used for excitation rather than the third. The oscillator strengths for these lines are many times larger than the oscillator strengths for the third-resonance lines. Table I shows that the signal strengths, i.e., the percentage change in the polarization of the detected fluorescent light at the resonance, is very low for the case of the first excited S states. This is due to at least three different factors. First, the additional step in the cascading process can decrease the signal strengths. Second, the lifetimes of these states are about a factor of 2 shorter than those for the second excited S states.<sup>17</sup> Therefore, larger rf magnetic fields are required to saturate these transitions. Finally, only a fraction of the total number of atoms that contribute to the observed fluorescent  $D_2$  light cascade via the S state. For example, in the case of the  $6^2S_{1/2}$  state of rubidium, only about 60% of the  $D_2$  light is contributed by atoms which decay via the  $6P_{1/2,3/2} \rightarrow 6S_{1/2} \rightarrow 5P_{3/2} \rightarrow 5S_{1/2}$  route, while 40% of this light comes from the  $6P_{3/2} \rightarrow 4D_{5/2} \rightarrow 5P_{3/2} \rightarrow 5S_{1/2}$  and  $6P_{1/2} \rightarrow 4D_{3/2} \rightarrow 5P_{3/2} \rightarrow 5S_{1/2}$  routes.<sup>17</sup> Of course, the fluorescence emitted by atoms that decay via different routes can have different degrees of polarization.

In Fig. 13 data for the third excited S states of  $Rb^{85}$ ,  $Rb^{87}$ , and  $Cs^{133}$  are shown. We observe very noisy signals in the case of the third excited S states due to the very low pumping rates for these states. This is because the oscillator strengths for the fourth-resonance lines are very much weaker than those for the third- and second-resonance lines. Moreover, we had to collect the data with the cell temperature lower than that for the case of second excited S states (Table I), resulting in a further decrease in the fluorescent-light intensity. It was necessary to operate at low temperatures due to collisional depolarization in the excited states. Our observations seem to indicate that the collisional depolarization cross sections are higher in the higher excited states.<sup>6</sup> Each of the resonance curves shown in Fig. 13 is a result of approximately 8 to 10 hours of signal averaging. The signal strengths of these resonances shown in Table I are only estimated strengths, as we had to use large zero-offsets on the lock-in amplifier for technical reasons.

We have not attempted to measure the hfs of the third excited S state ( $7^2S_{1/2}$ ) of potassium due to

the difficulty in separating the  $5802\text{-}\text{\AA}$  ( $7S_{1/2} \rightarrow 4P_{3/2}$ ) radiation from the  $5783\text{-}\text{\AA}$  ( $7S_{1/2} \rightarrow 4P_{1/2}$ ) radiation by broadband interference filters. We must use broadband filters if a large solid angle of detection is desired. It is necessary to filter out one or the other of the two fine-structure components in order to be able to monitor the electronic polarization of the  $7^2S_{1/2}$  state by observing the  $5802\text{-}\text{\AA}$  or  $5783\text{-}\text{\AA}$  fluorescent light. This limitation of fluorescence monitoring for the  $S_{1/2}$  states is discussed in detail in GCH.

The resonances shown in Figs. 8–13 are seen to be sitting on sloping base lines. These sloping base lines are due to a combination of two effects. The first of these is the decoupling of electronic and nuclear angular momenta. Secondly, the gain of the photomultiplier tube is affected slightly by the sweeping magnetic field. In some cases, there may also be some small effect of the change in the temperature of the cell and consequent change in the intensity of the fluorescent light during the run. The effect of the scanning of the photomultiplier tube gain by the magnetic field and that of the possible drifts in the temperature of the cell can, of course, be eliminated by normalizing the lock-in amplifier signal by the total fluorescent intensity, which we constantly record during the run. We have, however, not done so whenever the slopes of the base lines were very small (in all

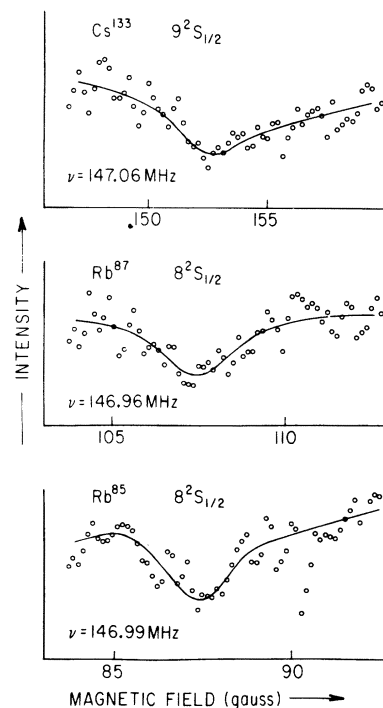


FIG. 13. rf resonance curves for the third excited state of  $Cs^{133}$ ,  $Rb^{87}$ , and  $Rb^{85}$ .

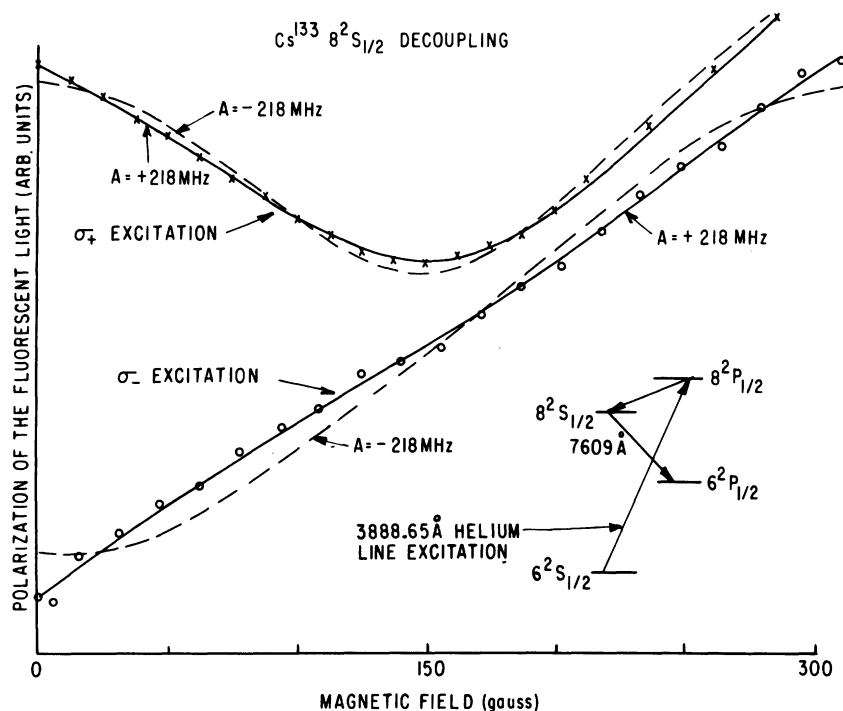


FIG. 14. Variation of the polarization of the 7609-Å fluorescent light (circles and crosses) in an external magnetic field due to the decoupling of the electronic and nuclear angular momenta. The lines are the least-squares fits to the experimental data for both the positive and the negative values of the magnetic dipole coupling constant  $A$ . A positive value of  $A$  fits the experimental data much better than a negative value. A coincidence between the cesium ( $6^2S_{1/2} - 8^2P_{1/2}$ ) transition frequency and a strong helium 3888.6-Å line has been used for excitation in this particular case.

TABLE II. Table of the experimental and theoretical values of the hyperfine-structure coupling constant  $A$ .

| Isotope           | State        | $A_{\text{expt}}$ (MHz) | SE     | $A_{\text{theor}}$ (MHz) |                    |                      | RHF + CP <sup>c</sup>      | RHF + RCP <sup>b</sup> | SEMP <sup>e</sup> |
|-------------------|--------------|-------------------------|--------|--------------------------|--------------------|----------------------|----------------------------|------------------------|-------------------|
|                   |              |                         |        | RL <sup>b</sup> HF       | RL <sup>b</sup> HS | RL <sup>b</sup> OHFS |                            |                        |                   |
| Na <sup>23</sup>  | $3^2S_{1/2}$ | 885.8                   | 996.4  | 631.1                    | 840.87             | 814.1                | 777.54, 857.8 <sup>d</sup> | 774.41                 |                   |
|                   | $4^2S_{1/2}$ | 202(3) <sup>a</sup>     | 228.45 | 151.8                    | 199.8              | 198.9                |                            |                        |                   |
| K <sup>39</sup>   | $4^2S_{1/2}$ | 230.85                  | 248.3  | 150.9                    | 222.0              | 196.6                | 184.49                     | 187.79                 |                   |
|                   | $5^2S_{1/2}$ | 55.50(60)               | 59.98  | 39.76                    | 56.57              | 53.42                |                            |                        |                   |
|                   | $6^2S_{1/2}$ | 21.81(18)               | 23.62  | 16.15                    | 22.38              | 21.72                |                            |                        |                   |
| K <sup>41</sup>   | $4^2S_{1/2}$ | 127.00                  | 136.0  | 82.94                    | 122.0              | 108.1                | 101.40                     | 103.21                 |                   |
|                   | $5^2S_{1/2}$ | 30.75(75)               | 32.85  | 21.85                    | 31.09              | 29.36                |                            |                        |                   |
|                   | $6^2S_{1/2}$ | 12.03(40)               | 12.99  | 8.876                    | 12.30              | 11.94                |                            |                        |                   |
| Rb <sup>85</sup>  | $5^2S_{1/2}$ | 1011.9                  | 1084.8 | 668.6                    | 1003               | 856.9                | 793.54                     | 821.3                  |                   |
|                   | $6^2S_{1/2}$ | 239.3(1.2)              | 261.6  | 176.1                    | 254.5              | 237.5                |                            |                        |                   |
|                   | $7^2S_{1/2}$ | 94.00(64)               | 103.9  | 71.23                    | 101.3              | 97.58                |                            |                        |                   |
|                   | $8^2S_{1/2}$ | 45.5(2.0)               | 51.6   | 36.15                    | 50.78              | 49.25                |                            |                        |                   |
| Rb <sup>87</sup>  | $5^2S_{1/2}$ | 3417.3                  | 3675.6 | 2266                     | 3398               | 2904                 | 2689.4                     | 2783.4                 |                   |
|                   | $6^2S_{1/2}$ | 809.1(5.0)              | 885.6  | 596.7                    | 862.5              | 804.8                |                            |                        |                   |
|                   | $7^2S_{1/2}$ | 318.1(3.2)              | 351.6  | 241.4                    | 343.4              | 330.7                |                            |                        |                   |
|                   | $8^2S_{1/2}$ | 158.0(3.0)              | 174.9  | 122.5                    | 172.1              | 166.9                |                            |                        |                   |
| Cs <sup>133</sup> | $6^2S_{1/2}$ | 2298.1                  | 2342.3 | 1519                     | 2289               | 1763                 | 1683.45                    | 1854.3                 | 2449.8            |
|                   | $7^2S_{1/2}$ | 546.3(3.0)              | 570.8  | 412.5                    | 591.7              | 516.0                |                            |                        | 579.8             |
|                   | $8^2S_{1/2}$ | 218.9(1.6)              | 230.5  | 172.1                    | 239.3              | 218.1                |                            |                        | 231.9             |
|                   | $9^2S_{1/2}$ | 109.5(2.0)              | 115.8  | 87.55                    | 120.9              | 112.0                |                            |                        | 116.3             |

<sup>a</sup> K. H. Liao *et al.*, following paper, Phys. Rev. A **8**, 2811 (1973).

<sup>b</sup> A. Rosén and I. Lindgren, Physica Scripta **6**, 109 (1972).

<sup>c</sup> L. Tterlikkis, S. D. Mahanti, and T. P. Das, Phys. Rev. **176**, 10 (1968).

<sup>d</sup> T. Lee, N. C. Dutta, and T. P. Das, Phys. Rev. A **1**, 995 (1970).

<sup>e</sup> D. W. Norcross, Phys. Rev. A **7**, 606 (1973).

cases except for the  $7^2S_{1/2}$  state of  $\text{Cs}^{133}$ ) compared to the magnitude of the observed resonance signal. We have, of course, corrected for the shift in the position of the observed resonance due to the sloping base lines.

We have listed the theoretical lifetimes of the states that we have investigated in column 7 of Table I. These lifetimes have been evaluated by Coloumb approximation. The widths of the observed resonance curves are consistent with these lifetimes. However, we have not tried to analyze our data for the lifetime of these states, as we are now investigating the lifetimes of these states by the cascade-Hanle effect, and we expect to get much better lifetime measurements by this method.

The sign of the magnetic dipole coupling constant  $A$  cannot be determined from the position of the S-state resonance, as this is independent of the sign of  $A$ . The hfs of the S states is almost entirely due to the contact interaction with the valence electrons. The core-polarization contribution to the hfs in the ground states is calculated to be of the order of 10 to 20% of the experimental value.<sup>18</sup> Therefore,  $A$  values for the S states are almost certainly positive. We have, however, ascertained that this is indeed so for two states. If the sign of  $A$  were negative for the  $7^2S_{1/2}$  state of Rb, the intensity ratios of the four  $7^2P_{3/2}$  resonances would have been different. Another convenient method of determining the sign of  $A$  is by decoupling spectroscopy.<sup>6</sup> Our decoupling data for the  $8^2S_{1/2}$  state of  $\text{Cs}^{133}$  are shown in Fig. 14. Here, the change in the circular polarization of the  $7609\text{-}\text{\AA}$  ( $8S_{1/2} \rightarrow 6P_{1/2}$ ) fluorescent light due to the decoupling of electronic and nuclear angular momenta in an external magnetic field is observed.

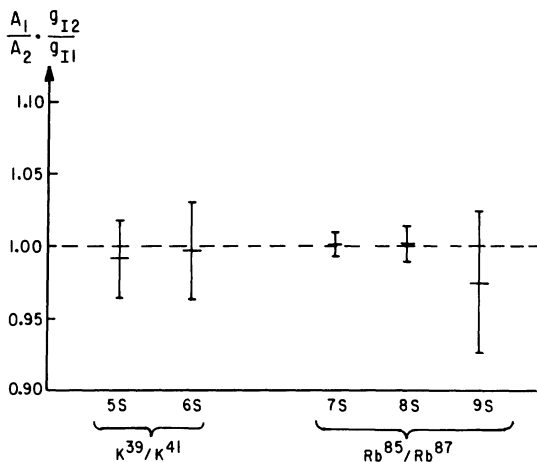


FIG. 15. Diagram showing the consistency of our results for different isotopes of potassium and rubidium. The isotopes are labeled by subscripts 1 and 2.

The exciting light in this case was the helium 3888- $\text{\AA}$  line, which accidentally coincides with the  $\text{Cs}(6S_{1/2} \rightarrow 8P_{1/2})$  transition. With helium light excitation, the change in the shape of the decoupling curve for different signs of  $A$  is much more noticeable than with the resonance light excitation. This is due to the nonwhite excitation of the  $8^2P_{1/2}$  state. The circles and crosses in Fig. 14 are the experimental points for two different senses of circular polarization of the exciting light. The lines are the least-squares fit to these data, with  $A = +218$  and  $-218$  Mhz. It is clear that only the positive value of the magnetic dipole coupling constant  $A$  fits the data. Although we have not checked the sign of the magnetic dipole coupling constants  $A$  for every state reported on in this paper, we believe that our assignment of positive signs to all these states is correct.

Our results are listed in Table II. The error bars, in most cases, are based on a statistical analysis of the results of several runs. Each resonance for the first and second excited S states has been repeated about 6 to 8 times. The error bars represent two standard deviations in the statistical spread of the results plus generous allowances for such effects as errors in the cali-

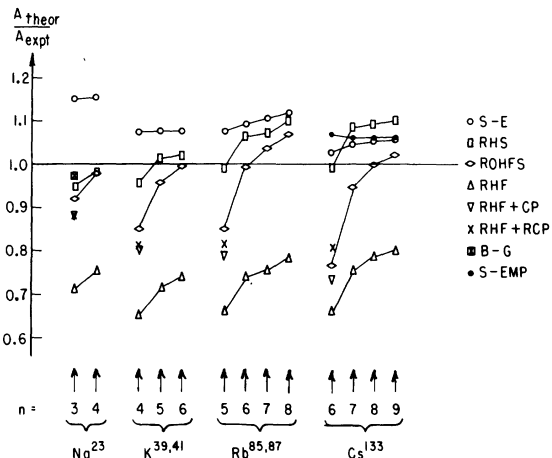


FIG. 16. A pictorial representation of our experimental results and some of the theoretical values of the hyperfine interaction constant  $A$ . Ratios of the experimental and theoretical values of  $A$  have been plotted against the principal quantum numbers of the states. SE represents the results of the semiempirical formula, while RHS, RHF, and ROHFS represent the relativistic Hartree-Slater, Hartree-Fock, and optimized Hartree-Fock-Slater schemes, respectively. RHF-CP is the result of the relativistic Hartree-Fock method, including core-polarization effects. RHF-RCP represents the RHF-CP results corrected for relativistic effects in the core-polarization term. BG is the result of the Brueckner-Goldstone many-body perturbation theory. SEMP stands for the results of a semiempirical model potential.



bration of the Helmholtz coils (which was done by optical pumping), errors in the correction for sloping base lines, etc. We have taken only about two curves each for the third excited states, owing to the long integration times involved. Here, the assignment of the error bars is somewhat arbitrary; however, we believe that the correct value lies well within the assigned error bars. We have assigned the error bars to the hfs values of two different isotopes completely independent of each other. Since the hyperfine anomaly should be much smaller than the accuracy of the present measurements, one can, perhaps, deduce better  $A$  values for these states by scaling the  $A$  values for the two isotopes by their  $g_I$  factors and comparing. The consistency of our results for the two isotopes of rubidium and potassium shows that perhaps our measurements are better than the indicated error bars (see Fig. 15). Here, the ratio  $A_1 g_{I2}/A_2 g_{I1}$  has been plotted against the principal quantum numbers of the states for the two isotopes of potassium and rubidium. This ratio, in the absence of hyperfine anomalies, should be unity.

## V. DISCUSSION

In this section we will compare our experimental results with some of the theoretical values of  $A$  that are available. Recently, Rosén and Lindgren<sup>7</sup> have calculated hfs coupling constants using restricted self-consistent-field methods for the sequences of  $S$  and  $P$  states of alkali-metal atoms. Also, Norcross<sup>16</sup> has calculated the  $A$  values for the 6, 7, 8, and 9  $S$  states of cesium using a semiempirical model potential. Both of these calculations, as well as the results obtained from the semiempirical formula for  $S$  states,<sup>11</sup> allow us to compare the experimental and the theoretical  $A$  values for sequences of  $S$  states. Some interesting conclusions can be drawn from these comparisons.

For completeness, we have included in Table II the well-known ground-state hfs constants of the alkali-metal atoms. We have also included the hfs value for the  $4^2S_{1/2}$  state of sodium.<sup>19</sup> Columns 4–10 of the table list some of the theoretical  $A$  values. Column 4 gives the values of the magnetic dipole coupling constants calculated from the semiempirical formula<sup>11</sup>

$$A = \frac{8}{3} \frac{cR_\infty \alpha^2 Z g_I}{n_0^3} \left( 1 - \frac{d\sigma}{dn} \right) F_r(j, Z) (1 - \epsilon) (1 - \delta). \quad (47)$$

Here,  $n_0$  is the effective principal quantum number of the state,  $\sigma$  is the Rydberg correction,  $F_r(j, Z)$

is the relativistic correction, and  $\epsilon$  and  $\delta$  are the corrections which are required due to the distributions of the nuclear magnetic moment and the nuclear charge over the nuclear volume, respectively. All other symbols in Eq. (47) have their usual meaning. Both the effective quantum number  $n_0$  and the quantity  $d\sigma/dn$  are deduced from the measured binding energies of the atomic states.<sup>20</sup> We have used the values of the correction terms  $F_r(j, Z)$ ,  $\epsilon$ , and  $\delta$  which are listed in Kopfermann.<sup>11</sup> Columns 5, 6, and 7 of Table II give the  $A$  values calculated by Rosén and Lindgren using relativistic Hartree-Fock, Hartree-Slater, and optimized Hartree-Fock-Slater schemes, respectively. Column 8 shows the  $A$  values calculated by Tterlikkis *et al.*<sup>19</sup> They have taken into account both the core-polarization and the relativistic effects, the former by a moment-perturbation procedure and the latter by a relativistic Hartree-Fock method. These calculations have been done only for the ground state of the alkali-metal atoms. The ground-state hfs of sodium has also been calculated using the Brueckner-Goldstone many-body perturbation theory by Lee *et al.*<sup>21</sup> (also shown in column 8). The calculation of Tterlikkis *et al.* does not take into account the relativistic effects in the core-polarization term itself. Rosén and

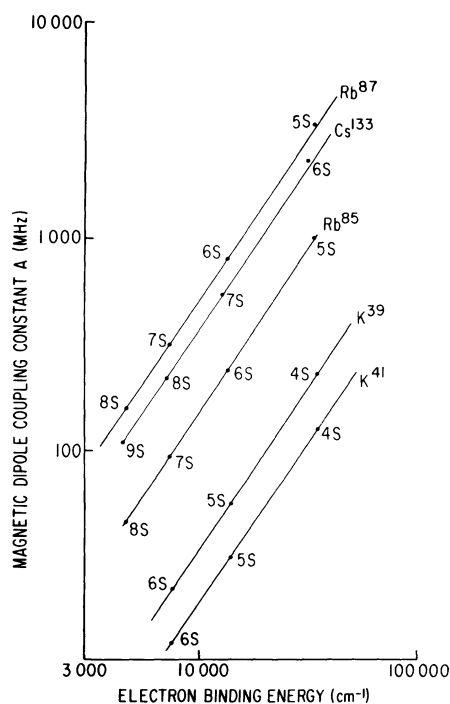


FIG. 17. A plot of the experimental values of the hfs coupling constant  $A$  for various  $S$  states of alkali atoms against the valence electron binding energies on a log-log scale.

Lindgren have applied a relativistic correction to the Tterlikkis *et al.* core-polarization term, and the resulting  $A$  values are shown in column 9. The results of Norcross's<sup>16</sup> calculations using a semiempirical model potential are shown in column 10. In this calculation, two parameters in the model potential were chosen such that the spectroscopic term values of the  $6^2S$  and the  $6^2P$  states of Cs agree with those calculated using this potential. A graphical summary of the results of various calculations is shown in Fig. 16. The ratio of the theoretical and experimental  $A$  values has been plotted against the principal quantum numbers for various states. Referring to Fig. 16, the following observations can be made.

The values of  $A$  calculated by the semiempirical formula always lie higher than the experimental values. If Rosén-Lindgren relativistic correction factors are used instead of those of Kopfermann, the theoretical  $A$  values will be even higher; i.e., the disagreement between the theoretical and experimental values will increase. Considering the simplicity and generality of the semiempirical formula, the agreement with the experimental values that this formula provides (within about 10%) is remarkable. The semiempirical formula predicts that the hfs constant  $A$  is proportional to the  $\frac{3}{2}$  power of the binding energy of the valence electron in that state, if the small term  $d\sigma/dn$  is neglected. In Fig. 17, we have plotted  $\log A_{\text{expt}}$  against  $\log E$ , where  $E$  is the binding energy of the valence electron. All the experimental points for various alkali-metal isotopes are seen to lie on parallel straight lines as expected. In all cases the ground-state  $A$  values lie somewhat higher. It is interesting to note, however, that this small discrepancy is in the same direction as one would expect as a result of neglect of the  $d\sigma/dn$  term.

Of the restricted self-consistent-field methods, the relativistic Hartree-Slater scheme gives the best agreement with the experimental  $A$  values, and the over-all agreement is very good. It is worth noting that Rosén and Lindgren have not explicitly taken the core polarization into account, as their principal aim was to calculate new and more accurate relativistic correction factors for  $^2S$  and  $^2P$  states. Inclusion of core polarization explicitly will perhaps move all these theoretical hfs values somewhat higher. It is interesting that the ratio  $A_{\text{theor}}/A_{\text{expt}}$  systematically increases with increasing principal quantum number for all alkali-metal atoms that we have investigated and for all three schemes that Rosén and Lindgren have used. In Fig. 18 we have plotted the ratio of the theoretical binding energies calculated by Rosén and Lindgren using the relativistic Hartree-Fock, Hartree-Slater, and the optimized Hartree-

Fock-Slater schemes to the experimental ones. It is very interesting that the ratios of the theoretical and experimental binding energies have exactly the same trend with the principal quantum number  $n$  as do the ratios of the theoretical and experimental hfs coupling constants  $A$ .

The Tterlikkis *et al.*  $A$  values for the ground state, calculated by the relativistic Hartree-Fock method and including core-polarization effects, are small compared to the experimental values. If the relativistic correction is applied to the core-polarization term,<sup>7</sup> the resulting  $A$  values are seen to agree better with the experimental values. The Lee *et al.*  $A$  value for the ground state of sodium, calculated by the Brueckner-Goldstone many-body perturbation theory, agrees very well with the experiment. This may indicate that electron correlation effects are quite important for S-state hyperfine structure. An obvious question, however, is how well similar Brueckner-Goldstone calculations would work for the higher S states of sodium and for the S states of the other alkali atoms. Would the inclusion of electron correlation effects remove the striking increase in  $A_{\text{theor}}/A_{\text{expt}}$  with principal quantum number?

The results of Norcross's calculations for the S states of Cs using a semiempirical model potential agree very well with the experimental values. It is remarkable that the ratio of Norcross's values to the experimental values is nearly independent of the principal quantum number, in striking contrast to the results of the self-consistent-field calculations.

In summary, although many creditable attempts

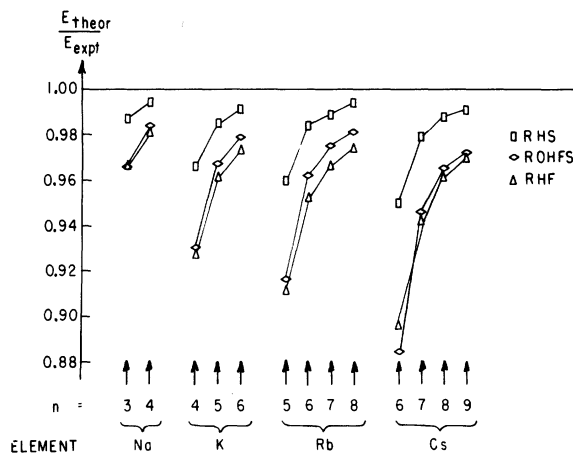


FIG. 18. A plot of the ratio of the theoretical and experimental binding energies for the valence electrons against their principal quantum numbers for various alkali-metal atoms. RHS, ROHFS, and RHF stand for the relativistic Hartree-Slater, optimized Hartree-Fock-Slater, and Hartree-Fock schemes, respectively.

have been made to calculate the S-state hfs intervals of alkali atoms, no really precise theory seems to exist yet. Theories such as those of Rosén and Lindgren which predict the hfs intervals for several excited S states in each alkali atom would seem particularly valuable now that systematic experimental measurements are available for comparison. It seems clear that further theoretical work would be very useful at this time.

## ACKNOWLEDGMENTS

We are grateful to Dr. S. Chang for his help in the initial stages of this work. Our thanks are also due to Dr. B. R. Bulos for help with rf circuits and to Dr. W. Nagourney for help with a PDP-8/S computer during the early stages of this experiment. We are thankful to C. Tai for making a least-squares fit of the Cs  $8^2S_{1/2}$  decoupling data.

\*Work supported in part by the Joint Services Electronics Program (U. S. Army, U. S. Navy, and U. S. Air Force) under Contract No. DAAB07-69-C-0383, and in part by the U. S. Air Force Office of Scientific Research under Contract No. AFOSR-72-2180.

†Permanent address: Department of Physics, Chalmers University of Technology, Fack, S-40220, Göteborg, Sweden.

‡Supported in part by the Swedish Natural Science Research Council.

<sup>1</sup>J. Brossel and F. Bitter, *Phys. Rev.* **86**, 308 (1952); A. Kastler and J. Brossel, *Compt. Rend.* **229**, 1213 (1949).

<sup>2</sup>F. D. Colgrove, P. A. Franken, R. R. Lewis, and R. H. Sands, *Phys. Rev. Lett.* **3**, 420 (1959); P. A. Franken, *Phys. Rev.* **121**, 508 (1961).

<sup>3</sup>G. zu Putlitz, in *Atomic Physics* (Plenum, New York, 1969).

<sup>4</sup>S. Chang, R. Gupta, and W. Happer, *Phys. Rev. Lett.* **27**, 1036 (1971).

<sup>5</sup>R. Gupta, S. Chang, C. Tai, and W. Happer, *Phys. Rev. Lett.* **29**, 695 (1972).

<sup>6</sup>R. Gupta, S. Chang, and W. Happer, *Phys. Rev. A* **6**, 529 (1972).

<sup>7</sup>A. Rosén and I. Lindgren, *Physica Scripta* **6**, 109 (1972).

<sup>8</sup>B. P. Kibble and S. Pancharatnam, *Proc. Phys. Soc.*

(London) **86**, 1351 (1965); W. Hanle, R. Pepperl, and H. Reuscher, *Physics of One- and Two-Electron Atoms* (North-Holland, Amsterdam, 1969), p. 375; R. L. Smith and T. G. Eck, *Phys. Rev. A* **2**, 2179 (1970).

<sup>9</sup>S. Svanberg, P. Tsekeris, and W. Happer, *Phys. Rev. Lett.* **30**, 817 (1973).

<sup>10</sup>G. W. Series, *Rep. Prog. Phys.* **22**, 280 (1959).

<sup>11</sup>H. Kopfermann, *Nuclear Moments* (Academic, New York, 1968).

<sup>12</sup>L. K. Lam, R. Gupta, and W. Happer, *Bull. Am. Phys. Soc.* **18**, 121 (1973).

<sup>13</sup>F. Bloch and A. Siegert, *Phys. Rev.* **57**, 522 (1940).

<sup>14</sup>S. C. Brown, *Introduction to Electrical Discharges in Gases* (Wiley, New York, 1966).

<sup>15</sup>G. zu Putlitz, *Comments At. Mol. Phys.* **1**, 51 (1969).

<sup>16</sup>D. W. Norcross, *Phys. Rev. A* **7**, 606 (1973).

<sup>17</sup>O. S. Heavens, *J. Opt. Soc. Am.* **51**, 1058 (1961).

<sup>18</sup>L. Tterlikids, S. D. Mahanti, and T. P. Das, *Phys. Rev.* **176**, 10 (1968).

<sup>19</sup>K. H. Liao, R. Gupta, and W. Happer, following paper *Phys. Rev. A* **8**, 2811 (1973).

<sup>20</sup>C. E. Moore, NBS Circular No. 467 (U. S. GPO, Washington, D. C. ).

<sup>21</sup>T. Lee, N. C. Dutta, and T. P. Das, *Phys. Rev. A* **1**, 995 (1970).